1990-06

An investigation of the as-quenched and early aging characteristics of a Al - 4.1wt%Li binary alloy by X-ray diffraction

Fuller, Scott J.

Monterey, California: Naval Postgraduate School

(2)

NAVAL POSTGRADUATE SCHOOL
Monterey, California

THESIS

AN INVESTIGATION OF THE AS-QUENCHED AND EARLY AGING CHARACTERISTICS OF A AL - 4.1WT.% LI BINARY ALLOY BY X-RAY DIFFRACTION

by

Scott J. Fuller

June 1990

Thesis Advisor A.G. Fox

Unclassified

security classification of this page

REPORT DOCUMENTATION PAGE

1a Report Security Classification: Unclassified		1b Restricuve Markings	
2a Security Classification Authority		3 Distribution/Availability of Report: Approved for public release; distribution is unlimited.	
2b Declassification/Downgrading Schedule			
4 Performing Organization Report Number(s)		5 Monitoring Organization Report Number(s)	
6a Name of Performing Organization: Naval Postgraduate School	6b Office Symbol (*If applicable*) 33	7a Name of Monitoring Organization: Naval Postgraduate School	
6c Address (*city, state, and ZIP code*): Monterey, CA 93943-5000		7b Address (*city, state, and ZIP code*): Monterey, CA 93943-5000	
8a Name of Funding Sponsoring Organization	8b Office Symbol (*if applicable*)	9 Procurement Instrument Identification Number	
8c Address (*city, state, and ZIP code*)		10 Source of Funding Numbers	
		Program Element No	Project No / Task No / Work Unit Accession No

11 Title (*include security classification*)
AN INVESTIGATION OF THE AS-QUENCHED AND EARLY AGING CHARACTERISTICS OF A AL - 4.1WT.% LI BINARY ALLOY BY X-RAY DIFFRACTION

12 Personal Author(s) Scott J. Fuller

13a Type of Report	13b Time Covered	14 Date of Report (*year, month, day*)	15 Page Count
Master's Thesis	From To	June 1990	63

16 Supplementary Notation The views expressed in this thesis are those of the author and do not reflect the official policy or position of the Department of Defense or the U.S. Government.

17 Cosati Codes			18 Subject Terms (*continue on reverse if necessary and identify by block number*)
Field	Group	Subgroup	Aluminum-Lithium Alloys, Microstructural development

19 Abstract (*continue on reverse if necessary and identify by block number*)

The as-quenched and early aging characteristics of an as-cast, binary, Al - 4.1wt.% Li alloy has been studied by X-ray diffraction. Flat plate samples were solution heat treated at 540°C under argon and ice-brine quenched. Powder samples were made from flat plate samples in the as-quenched condition by filing at liquid nitrogen temperatures. Aging was conducted at 200°C on both plate and powder samples. The presence of very broadened 100 superlattice reflections of $\delta' Al_3Li$ ($L1_2$ structure) and small reflections of δ AlLi (B32 structure) were observed in the as-quenched condition for the plate sample. The powder sample showed the additional 110 superlattice peak of δ' and 220 δ peak. This clearly showed the preferred orientation effects of the plate. From the as-quenched powder, a volume fraction of 77% δ' with an average particle diameter of 53Å was calculated. Long range order parameter was calculated as 0.50, indicating an almost maximum degree of order in the as-quenched condition. These results indicate that the as-quenched alloy has 77% ordered regions of about 50Å surrounded by disordered matrix. Aging of both the powder and plate indicated that δ' particle growth follows Ostwald ripening. δ peaks were observed throughout the aging process. These results support the theory of an ordering transformation followed by a spinodal decomposition during and immediately following the quench.

20 Distribution/Availability of Abstract	21 Abstract Security Classification	
☒ unclassified/unlimited ☐ same as report ☐ DTIC users	Unclassified	
22a Name of Responsible Individual: A.G. Fox	22b Telephone (*include Area code*): (408) 663-3275	22c Office Symbol: 54SsME FX

DD FORM 1473,84 MAR 83 APR edition may be used until exhausted
All other editions are oosolete

security classification of this page

Approved for public release; distribution is unlimited.

An Investigation of the As-quenched and Early Aging Characteristics of a Al - 4.1wt.% Li Binary Alloy by X-ray Diffraction

by

Scott J. Fuller
Captain, United States Marine Corps
B.S.M.E., University of Idaho, 1984

Submitted in partial fulfillment of the
requirements for the degree of

MASTER OF SCIENCE IN MECHANICAL ENGINEERING

from the

NAVAL POSTGRADUATE SCHOOL
June 1990

Author: [redacted]
Scott J. Fuller

Approved by: [redacted]
A.G. Fox, Thesis Advisor

[redacted]
Anthony J. Healey, Chairman,
Department of Mechanical Engineering

ABSTRACT

The as-quenched and early aging characteristics of an as-cast, binary, Al - 4.1wt.% Li alloy has been studied by X-ray diffraction. Flat plate samples were solution heat treated at 540°C under argon and ice-brine quenched. Powder samples were made from flat plate samples in the as-quenched condition by filing at liquid nitrogen temperatures. Aging was conducted at 200°C on both plate and powder samples. The presence of very broadened 100 superlattice reflections of $\delta' Al_3Li$ ($L1_2$ structure) and small reflections of δ AlLi (B32 structure) were observed in the as-quenched condition for the plate sample. The powder sample showed the additional 110 superlattice peak of δ' and 220 δ peak. This clearly showed the preferred orientation effects of the plate. From the as-quenched powder, a volume fraction of 77% δ' with an average particle diameter of 53Å was calculated. Long range order parameter was calculated as 0.50, indicating an almost maximum degree of order in the as-quenched condition. These results indicate that the as-quenched alloy has 77% ordered regions of about 50Å surrounded by disordered matrix. Aging of both the powder and plate indicated that δ' particle growth follows Ostwald ripening. δ peaks were observed throughout the aging process. These results support the theory of an ordering transformation followed by a spinodal decomposition during and immediately following the quench.

TABLE OF CONTENTS

LIST OF TABLES

LIST OF FIGURES

I. INTRODUCTION

Aluminum-lithium alloys have received renewed interest in the past few years. These alloys have the potential of mechanical properties similar to current aluminum alloys yet with up to a 10% lower density and a 10-12% increase in the elastic modulus [Ref. 1]. This offers a weight savings that would be extremely valuable for many applications, especially the aerospace industry. Indeed, the current research and development of aluminum-lithium alloys is being driven by the need for the aluminum industry to improve their current alloys. As new advanced composites challenge the dominance of aluminum for use in aircraft production, the aluminum industry must develop better alloys to stay competitive.

The use of lithium as an alloying element to aluminum has long been considered. Unfortunately, the reduction in density and increase in strength is coupled with some deleterious properties such as a decrease in ductility and toughness. These problems have plagued the development of Al-Li alloys. Currently, there are now available some aluminum alloys that do have lithium alloyed into them. However, these current alloys are not capable of universally replacing all applications of conventional alloys. These alloys also are alloyed with two or more additional elements, thus reducing the major advantage of lithium addition.

The main efforts of recent research have been investigating the microstructural transformations occurring in Al-Li alloys. Most notably, the development and growth of the Al_3Li particle, usually called delta prime (δ'). This precipitate is the main strengthening agent in Al-Li alloys, yet its formation and development are far from being understood. It is hoped that through research this development can be characterized and lead to a more successful application of alloying with lithium.

Most recent investigations have been conducted using the transmission electron microscope (TEM). Whitman recently conducted X-ray diffraction of an Al-2.5%Li-0.15%Zr (by weight) alloy, and showed that precipitate size and subsequent growth can be tracked by X-ray diffraction [Ref. 2]. This study will concentrate solely on using X-ray diffraction of an as-cast, binary Al-4.1wt.%Li alloy, to investigate the early aging characteristics. Both plate and powder samples will be made from the alloy, and an aging sequence will be carried out on both. The powder sample will allow an investigation into the preferred orientation effects of the plate samples.

II. BACKGROUND

A. ALUMINUM-LITHIUM ALLOYS

1. Historical Development

Lithium is one of few elements that has a solid solubility in aluminum greater than 1 atomic percent, so it was naturally considered as a candidate for alloying with aluminum. This can be traced back to as early as 1919, and in the 1920's, the German alloy Scleron became the first commercial Al-Li based alloy [Ref. 3, p.71]. Many other combinations of lithium and various other elements alloyed with aluminum were soon developed, but the rapid improvements made in Al-Mg-Cu alloys at this time caused development of these Al-Li alloys to be hindered.

In 1942, a patent for an Al-Cu-Li-X alloy was granted to I. M. LeBaron of ALCOA, but it wasn't until 1958 that ALCOA developed alloy 2020 based on this system. Once again, the development of Al-Li alloys had received little attention due to the development of alloy 7075 in 1943, which became and still is a dominate commercial, high strength aluminum alloy. However, alloy 2020 did make an impression, and was used in 1958 for the U.S.Navy RA-5C Vigilante aircraft. Although considered a successful employment of an Al-Li alloy, the use of 2020 on the RA-5C did require special considerations in design and manufacture due to directional fracture toughness problems. This concern plagued the alloy, and the demand for 2020 never was great enough to warrant continued production. [Ref. 3, p.72]

The Soviet Union also developed Al-Li based alloys, and introduced an alloy designated 01420 in the late 1960's. Alloy 01420 was later used by the Russians in their MiG-25 aircraft [Ref. 4]. Up to this point, a thorough understanding of the microstructural transformations involved was never known. During the 1970's and continuing to the present, research has shifted to determine what transformations and strengthening mechanisms are occurring in these Al-Li alloys. The aluminum industry is accelerating the research and development of Al-Li alloys for a number of reasons. The need for lighter aircraft to conserve fuel and increase payload, continued advancements in composite materials, and current production successes will all contribute to continue the effort to achieve a better understanding and hence better employment of Al-Li alloys.

2. Advantages and Disadvantages of Al-Li Alloys.

The aluminum industry has many advantages in developing newer, stronger, and lighter aluminum alloys. Among them:

- There is an ample supply of lithium reserves that can be used for production of Al-Li alloys [Ref. 5].
- The engineering of aluminum alloys has a strong foundation based on years of experience. Al-Li alloys are emerging as overall well balanced aluminum alloys that will benefit from this experience. [Ref. 6]
- Current machinery and skill levels of the industry are well established and will allow for a rapid introduction of Al-Li alloys.
- Aluminum alloys, when compared to composites, have proven to provide a safer response to accidents, especially aircraft crashes. Composites tend to splinter, and given the increasing number of aircraft accidents occurring as the fleet of commercial aircraft ages, this is a major advantage to the aluminum industry. [Ref. 7]
- The possibility of super plasticity Al-Li alloys offers added incentive. Wadsworth et al. achieved a 1035% elongation of an Al-3Li-0.5Zr alloy [Ref. 8].

The aluminum industry's concerns for Al-Li alloys include:

- The low toughness problem, especially in the short transverse direction. Although the toughness problem is no longer as serious, it still must be improved upon.
- The low ductility of binary Al-Li alloys is a major disadvantage. It is hoped that further research will pinpoint the reasons for the low ductility.
- Current aluminum alloys enjoy success largely in part to their low cost. Al-Li alloys cost approximately three times as much, and this high cost is a major concern. This cost arises due to the extremely reactive and toxic nature of lithium, thus requiring special handling and production requirements [Ref. 9].
- Once in production, Al-Li scrap material will have to be kept separate from conventional aluminum scrap. This is a minor concern.

3. Current Alloys and Applications

The latest developments of Al-Li alloys include the 2090 and 8090 series of alloys. Table 1 on page 4 lists the compositions of the four current Al-Li alloys along with the two conventional 2024 and 7075 alloys. As can be seen in Table 1 on page 4, these current Al-Li alloys all include additional alloying elements, usually zirconium and copper. Zirconium and copper are usually added to improve the toughness and ductility. The additional phases that develop in alloys does not influence δ' formation, and significant amounts of copper or zirconium do not enter the δ' phase [Ref. 10]. Zirconium additions improve the toughness, stress corrosion resistance, and quench sensitivity by introducing Al_3Zr precipitates [Ref. 11]. These Al_3Zr precipitates are stable in precipitate

free zones of δ' near grain boundaries, thus reducing the grain boundary weakness in Al-Li alloys [Ref. 12].

Table 1. CONVENTIONAL AND ALUMINUM-LITHIUM ALLOY COMPOSITIONS (Nominal Weight %) [Ref.4]

alloy	Li	Cu	Mg	Mn	Zr	Zn	Cr
2090	2.2	2.8	--	--	0.1	--	--
8091	2.6	2.0	0.9	--	0.1	--	--
2091	2.0	2.2	1.5	--	0.1	--	--
8090	2.5	1.3	1.0	--	0.1	--	--
2024	--	4.4	1.5	0.6	--	--	--
7075	--	1.6	2.5	--	--	5.6	0.2

The above listed Al-Li base alloys are currently intended to be used on commercial applications for Boeing 7J7 aircraft, as well as other Boeing products, and also by the French Airbus Industrie for their A310, A320, and A300-600 [Refs. 7,13].

Uses for military applications are being tested. The U.S. Air Force is testing 8090 for use as a wing skin on an F15D aircraft. The first test flight was conducted in 1986, and a weight savings of 24 pounds coupled with increased panel performance and fatigue life shows promise [Ref. 14].

The U.S.Navy is also interested in the newer alloys, and is currently sponsoring, through the Naval Air Development Center in conjunction with ALCOA, a program for replacing conventional 7075 alloys with 2090 or 8090 series alloys. In particular, replacement of 7075-T6 with 2090-T8E41 for a maximum strength material, and replacement of 7075-T73 with either 2090 or 8092 for stress corrosion resistant materials. The Navy has also installed test panels on some ships and on some F/A-18 aircraft [Ref. 2, p.5].

B. MICROSTRUCTURE

1. Phase Descriptions

An Al-Li phase diagram is shown in Figure 1[Ref. 15]. The dashed lines represent the region that is still currently being investigated. For binary Al-Li alloys, in addition to the face centered cubic Al-Li solid solution phase (usually denoted as α), the other phases of concern are the body centered cubic Al-Li phase (δ), and the Al_3Li phase (δ').

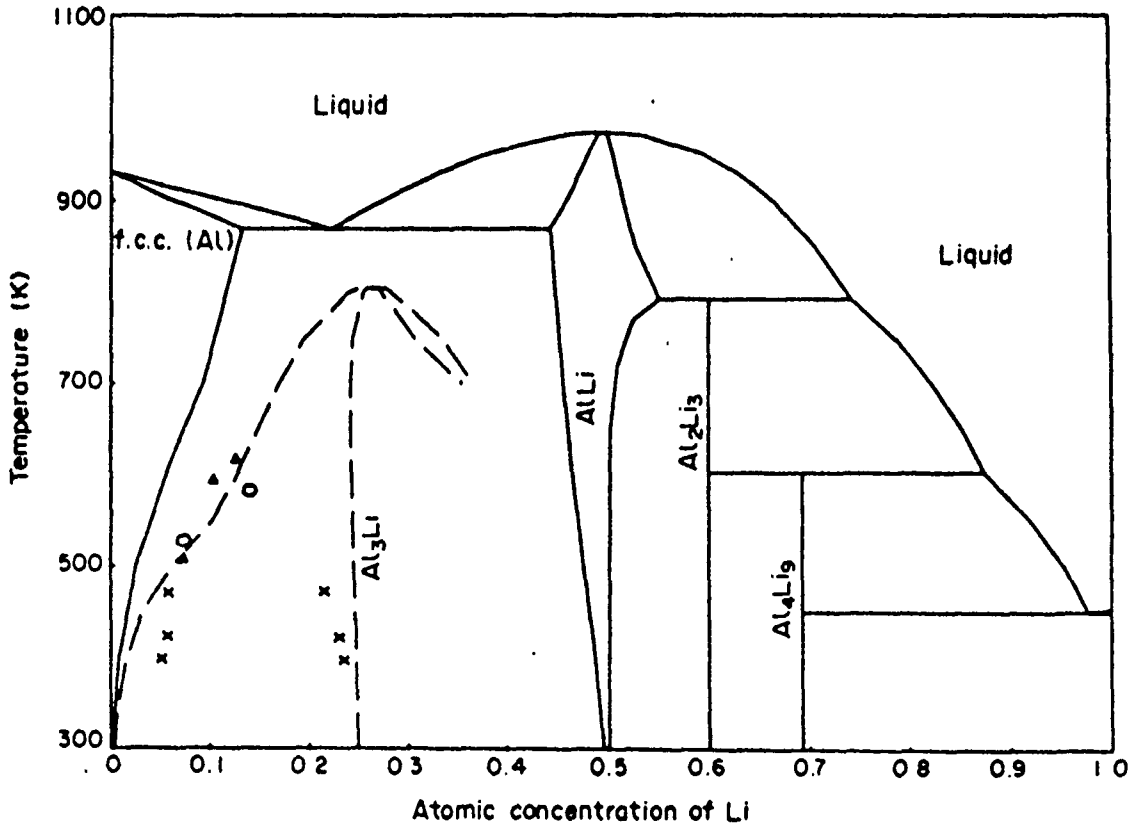

Figure 1. Al-Li Phase Diagram

a. δ Phase

The δ phase is a stable, intermetalic compound with a B32 (NaTl) type structure (see Figure 2). It has a lattice parameter of 6.38Å.

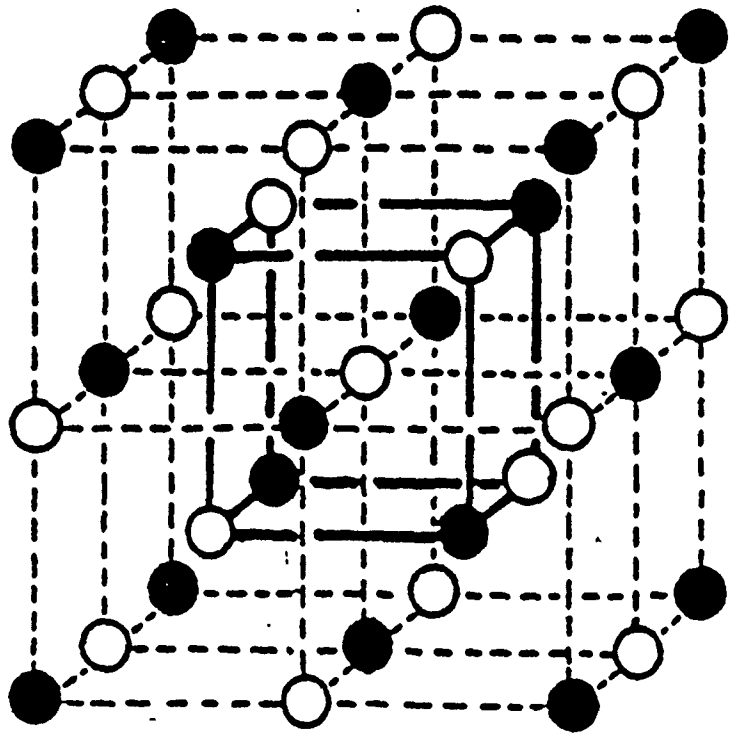

Figure 2. B32 Structure of δ Al-Li

The formation of δ is still being investigated. Niskanel et al suggested the process:

$$\alpha \rightarrow \delta' \rightarrow \delta$$

where δ formed from the preferential coarsening of δ' [Ref. 16]. Williams, however, proposed that δ forms independently of δ', nucleating heterogeneously on grain boundaries and also within the matrix [Ref. 17]. This δ formation is still usually considered to occur after the formation of δ', sometime during aging. Liu and Williams report that there is no apparent δ formation in alloys they tested even after 4 months of artificial aging [Ref. 18]. Cocco et al. reported they aged Al-Li alloys in such a way as to promote δ' precipitation while avoiding δ precipitation [Ref. 19]. Whitman, however,

has observed δ in the as-quenched state for his alloy [Ref. 2]. δ has also been observed to form at high angle grain boundaries in the early stages of aging [Ref. 20].

The growth of δ has been shown to occur in conjunction with the growth of δ' precipitate free zones (PFZ's). PFZ's form at the grain boundary, which is also a nucleation site for the δ particles. The dissolution of δ' particles in this region supports the growth of the PFZ. Indeed, Radmilovic et al. have determined a loss of lithium in this region, indicating that the dissolution of the δ' particle is a result of a loss of lithium, most probably to the δ phase [Ref. 21].

b. δ' Phase

δ' is a face centered cubic, metastable phase, with an ordered $L1_2$ structure (see Figure 3), having a stoichiometric composition of Al_3Li. δ' has a cube/cube orientation relationship with the matrix, and is referred to as a superlattice. It has a lattice parameter of 4.045Å, which is almost identical to the α matrix lattice parameter. This results in a small misfit strain (less than 0.1%) and allows for homogeneously distributed, coherent, spherical δ' precipitates found in Al-Li alloys. [Refs. 22,23]

The process of formation of δ' is not clearly understood. Current theories will be discussed in the next section. δ' has been reported by numerous investigators to be present in the as-quenched state.

The growth of δ' follows Ostwald ripening kinetics, having a cubed radius growth proportional to time. The particle size distribution (PSD) of δ' has been studied and compared with the growth process. Using a Weibull distribution model, Gu et al described the PSDs of δ' for binary alloys. A symmetrical distribution is predicted for approximately a 3.8% (wt.) lithium alloy, with lithium concentration affecting the skewness of the distribution, and also the rate of particle coarsening. Increasing lithium content will increase rate of δ' coarsening. [Ref. 24] Other work of Gu et al. attempted to further model the growth process using various Ostwald theories. The Lifshitz-Slyozov Encounter Modified (LSEM) theory was the most accurate in modeling the PSD of δ', but assumed coalescence of particles and indicates anti-phase boundaries (APBs) should be found in δ' particles [Ref. 25].

2. Current Precipitation Theories

For alloys greater than 5.5 at.% Li, the formation of δ' occurs during the quench from a supersaturated state. Indeed, most TEM studies have observed superlattice reflections in the as-quenched state. These superlattice reflections were also detected by Radmilovic et al. using X-ray diffraction [Ref. 26]. These reflections

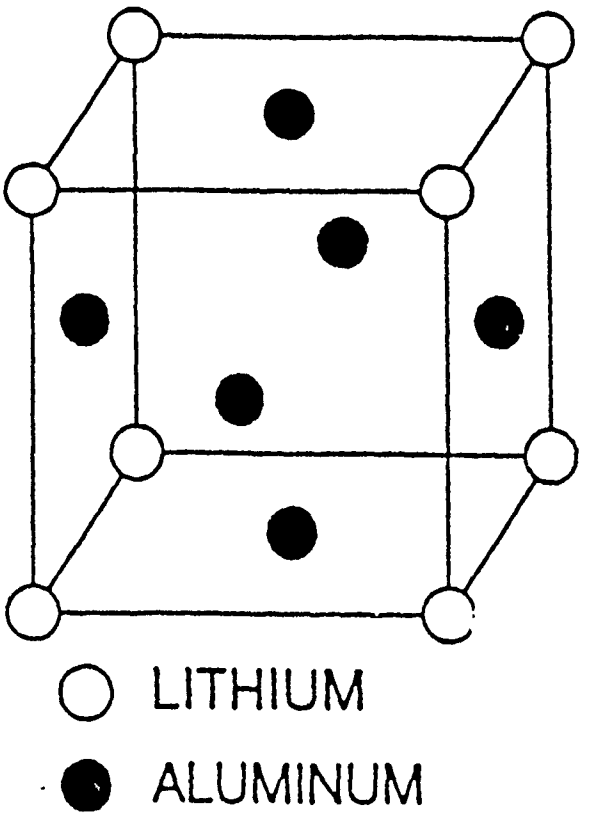

Figure 3. $L1_2$ Ordered Structure of δ' (Al_3Li)

correspond to ordered regions of δ' like precipitates. This region of interest in the Al-Li phase diagram of Figure 1 on page 5 is shown enlarged in Figure 4 on page 9.

Williams and Edington studied the δ' formation in 1975. They considered that δ' could form via conventional nucleation and growth or perhaps a spinodal decomposition. In attempting to determine if a spinodal were occuring, they concluded that although X-ray sideband structures should be seen, the fact that they were not could not disprove the spinodal theory due to the relatively weak intensities that these sidebands would have (1/600 of the fundamental) [Ref. 27].

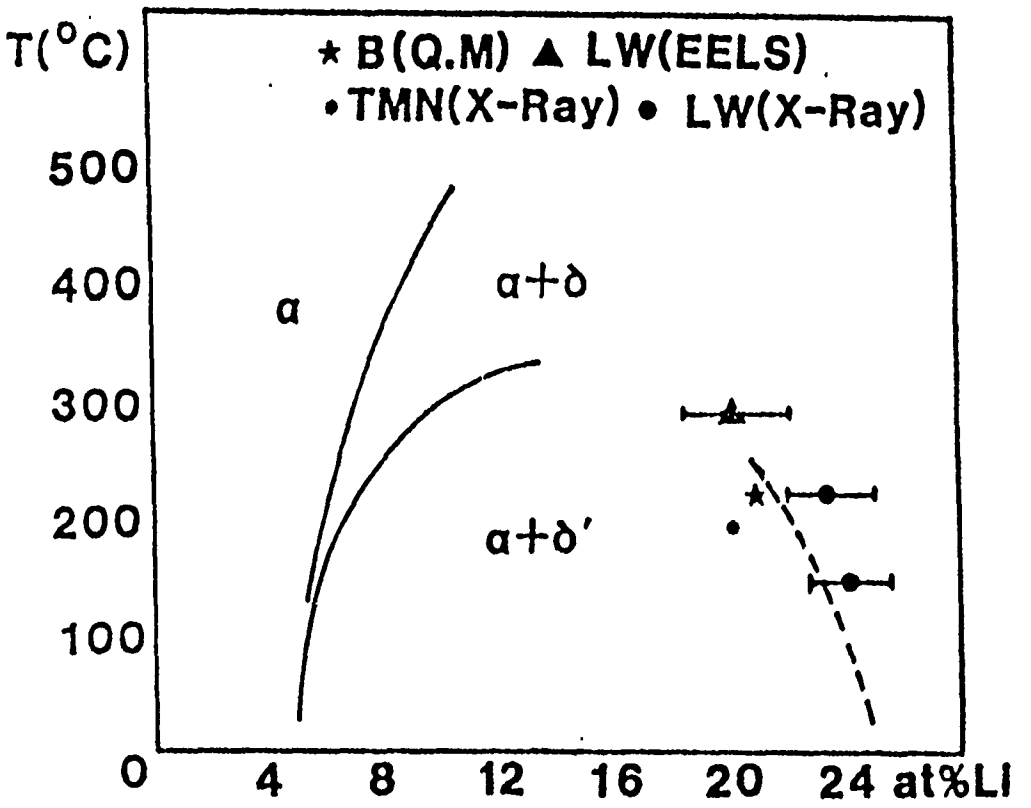

Figure 4. $\alpha + \delta'$ **Region of Al-Li Phase Diagram**

Sigli and Sanchez constructed a model based on the Cluster Variation Method (CVM). Their proposed phase diagram is shown in Figure 5. This diagram is in good agreement with the experimental data available, and predicts a miscibility gap within the α phase field. This suggests the formation of GP zones through either a spinodal decomposition or normal nucleation and growth, provided the formation of δ' can be avoided during the quench. However, most research has shown superlattice reflections associated with ordered regions of δ' after quenching. Also, to date, no one has been able to observe the formation of GP zones. [Ref. 28]

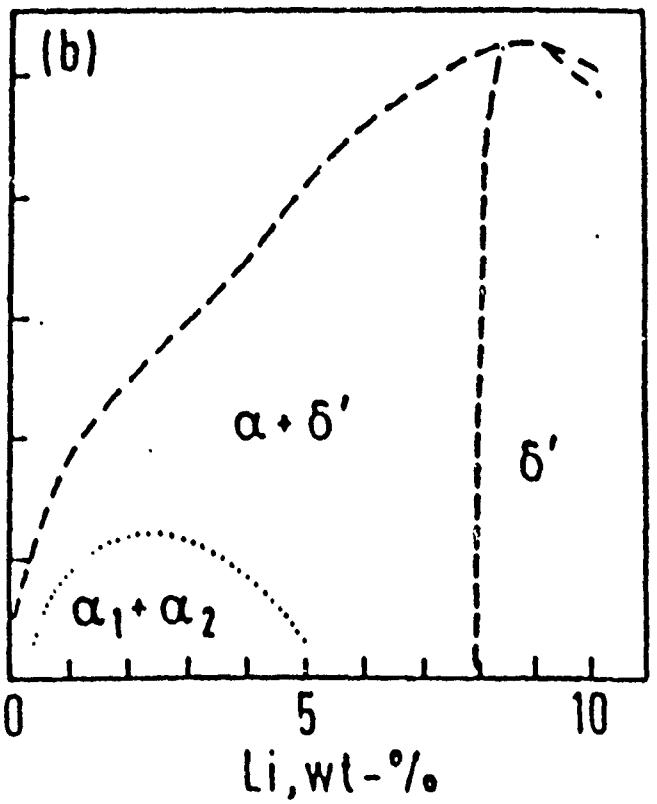

Figure 5. Proposed Miscibility Gap of Sigli and Sanchez

A theoretical model proposed by Khachaturyan et al. in 1986 offered a different δ' formation process. This process is shown in Figure 6 on page 11 Starting from a disordered solid solution at point A, this model predicts a congruent ordering process to point B. But point B, being unstable with respect to the spinodal, spinodally decomposes to point C.

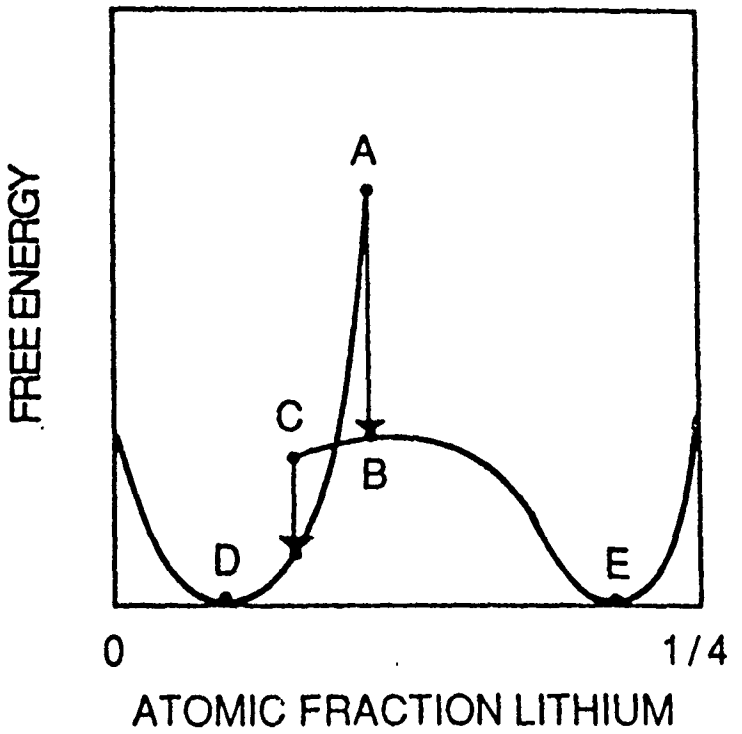

Figure 6. Spinodal Decomposition Model of Kachuturyan

C is now unstable, and disorders to D, which is the disordered matrix that is lithium lean. Point B also spinodally decomposes towards point E, which is the lithium rich ordered phase of δ' particles. [Ref. 29]

This theory predicts the existence of ordered regions in the as-quenched state. Sato et al. have imaged these ordered regions, as has Fox, by using high resolution electron microscopy (HREM). These ordered regions are easily distinguishable from the disordered regions, but are not recognizable as spherical δ' precipitates [Ref. 30].

Spooner et al. have also given evidence for a spinodal mechanism. Using small angle X-ray scattering (SAXS), they noted a rise and then fall in the δ' particle radius in early stages of aging. They suggested that a spinodal decomposition in the matrix occurred with fast coarsening, followed later by the nucleation of new, smaller δ' precipitates [Ref. 31, p.335]. Radmilovic et al. also concluded that Al-Li base alloys are ordered in the as-quenched state in support of this model [Ref. 26].

Chen et al. have also considered the phase equilibria of the binary Al-Li system. They calculated a metastable phase diagram from thermodynamic models for the δ'

phase. This is shown in Figure 7. Here, they consider the δ' phase to be a line compound [Ref. 32].

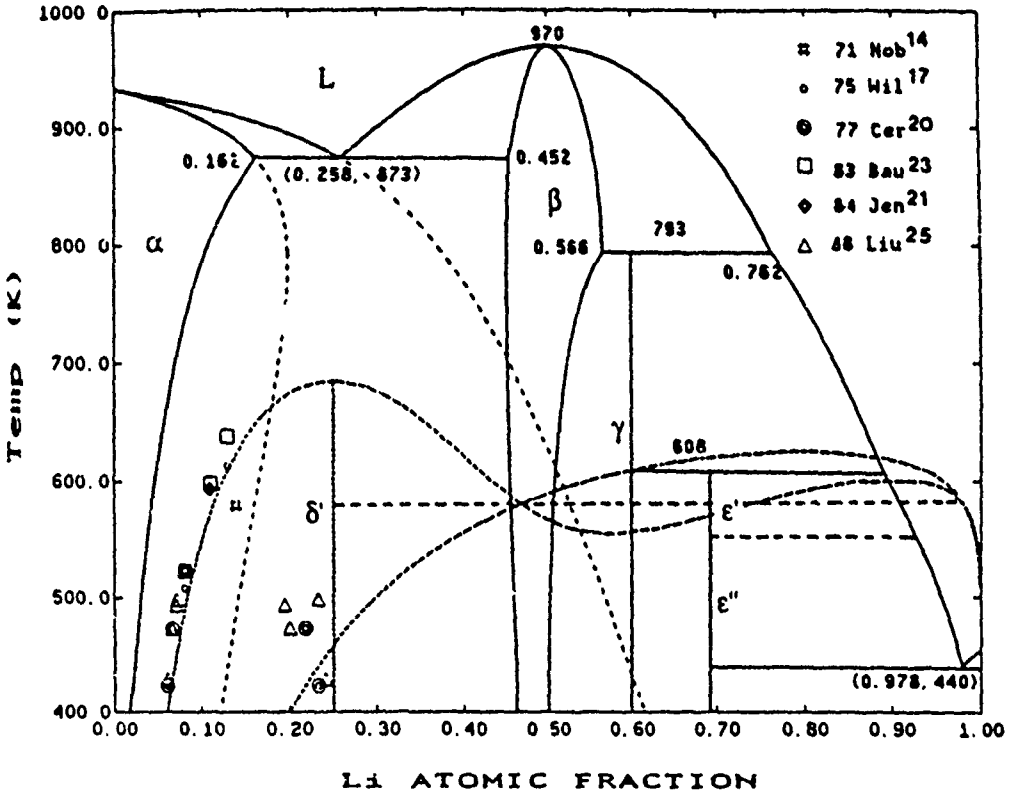

Figure 7. Al-Li Phase Diagram of Chen et al.

3. Phase Effects on Engineering Properties

a. Elastic Modulus

Al-Li alloys are significantly stiffer than pure aluminum. A 3% weight addition of lithium increases the specific modulus by about 30%. This was once thought to be due to δ' precipitation. Noble et al. showed that the modulus of elasticity is higher in as-quenched alloys and further aging only increases the modulus slightly [Ref. 33]. Sanders and Starke also concluded that the increase in elastic modulus with lithium content does not require the presence of the δ' phase [Ref. 34, p.931]. Fox and Fisher, noting that the nearest-neighbor (n.n.) distance in pure lithium is 3.031Å but only 2.86Å in Al-Li solid solution, theorized that the increase in modulus is due to the much

smaller volume for the valence electrons to occupy. This results in an increase in the force constant between n.n. lithium atoms in Al-Li alloys, which suggests a higher Debye temperature, and therefore a higher modulus of elasticity as lithium content increases [Refs. 35,36].

b. Strength

The increase in strength is due to the δ' precipitates, with a critical size of precipitate between 300-500Å for maximum strength [Refs. 37,38]. Noble et al. have studied the strengthening mechanisms for Al-Li alloys, which is dominated by the interaction between δ' particles and dislocations. They observed that the δ' particles are sheared by dislocations, leading to strengthening mainly by either the creation of APBs in the δ' (order hardening), or by a combination of order hardening and modulus hardening [Ref. 39].

Furukawa et al. explained the strengthening mechanism by modeling the movement of dislocations in pairs. They found that for underaged or peak-aged alloys, APBs and friction stresses of the matrix and δ' precipitates offered the main resistance to moving dislocations [Ref. 40].

c. Ductility and Toughness

The decrease in ductility and low fracture toughness are related to the increase in strength caused by the δ'. Sanders and Starke noted that when the coherent, ordered δ' particles are sheared by dislocations, work softening can occur. Once the δ' particles have been sheared, their resistance to further dislocation movement has decreased. This leads to strain localization, which is believed the primary reason for the ductility and fracture characteristics of Al-Li alloys. The decrease in ductility with increasing lithium content and aging time is associated with an increased tendency for planarity of slip. Sanders and Starke also observed that for short aging times, fracture occurs transgranularly, but for longer aging times, ductile fracture occurs intergranularly. [Refs. 41,34, p.934]

Furukawa et al. also observed dislocation pileup in low lithium alloys, indicating planar slip which can lead to low ductility. However, for alloys greater than 11 at.% lithium, this was not observed, and some other mechanism must be the origin of the low ductility. [Ref. 38]

4. Analysis Methods

There are many various experimental techniques employed to study the microstructure of metals. However, for Al-Li alloys, many difficulties arise that impede the study. As noted earlier, lithium is very reactive and toxic. The initially formed δ'

particles are extremely small and therefore difficult to observe. Finally, and perhaps the most limiting problem, is the difficulty in detecting the presence of lithium. Especially difficult is to quantitatively characterize the amount of lithium present. The benefits of quantitative analysis are many, with the possibilities of determining δ' stoichiometry and the binary phase diagram being just two. However, any quantitative technique should be capable of detecting less than 3 wt.% lithium, and have a spatial resolution of less than 500Å [Ref. 42,p.337]. Ideally, when dealing with Al-Li alloys, a spatial resolution of less than 50Å would be desired due to the extremely small size of the δ' precipitates and the presence of lithium.

In addition to quantitative techniques, there are many other qualitative techniques that are extremely valuable. A summary of some of the methods, both qualitative and quantitative, that have been attempted follows.

a. Electron energy loss spectroscopy (EELS).

EELS is a measure of the energy distribution of electrons as they emerge from a thin foil TEM sample. Chan and Williams have used ionization EELS and found a minimum detectable mass fraction of about 2.7% lithium [Ref. 43]. This sensitivity must be improved in order to detect lower lithium concentrations.

Plasmon loss EELs is a slightly different technique that could be employed, but it requires special equipment and acquiring and analyzing data is extremely time consuming [Ref. 42,p.340].

b. Convergent beam electron diffraction (CBED).

CBED can be used as an indirect method for detecting lithium. Sung et al. conducted CBED studies of Al-Li. Their results indicate a change in the δ' lattice parameter as a function of aging temperature, indicating a varying stoichiometry of δ'. They also conclude that due to the very small change in the lattice parameter, errors with this method must be improved upon before results can be confidently concluded. [Ref. 42,p.343]

c. Atom probe field ion microscopy (APFIM).

This is a technique that can effectively analyze all elements. Pickering reported successful imaging of δ', but noted further work was required to fully quantify lithium concentrations. This technique uses small volumes of samples, and is best employed concurrently with other methods (i.e. TEM). [Ref. 44]

d. Transmission electron microscopy (TEM).

The transmission electron microscope has seen extensive use for the study of Al-Li alloys. Unfortunately, the extremely small sample size can limit its use. The

presence of δ is often not detected by TEM in the early stages because of the reactive nature of this phase when preparing the TEM samples. Many investigators report the lack of δ based solely on the results of TEM observations, which is not necessarily definitive. Quantitative information is also difficult to obtain using TEM [Ref. 31, p.329].

e. X-ray diffraction (XRD).

XRD will not allow for any qualitative results of lithium content. However, the detection of the different phases, the ability to measure particle size and determine volume fraction, and the large sampling size, makes the XRD method an extremely valuable tool. This study will utilize XRD for these reasons.

C. PRINCIPLES OF X-RAY DIFFRACTION THEORY

X-ray diffraction (XRD) is based on the Bragg equation:

$$n\lambda = 2d\sin\theta \tag{1}$$

λ is the wavelength of incident radiation, θ is the angle of reflection, and d is the interplanar spacing. For a given plane (hkl), d is given as:

$$d = \frac{a_0}{\sqrt{h^2 + k^2 + l^2}} \tag{2}$$

Here, a_0 is the lattice parameter of the crystal structure. For any known compound and desired plane, d can easily be calculated, therefore θ can be determined for the location of diffraction intensities.

1. Factors affecting XRD

Many factors can affect the XRD results, most notably the observed intensity of the diffraction peak, and the broadening of the diffraction profile. Some of these factors will be discussed briefly.

a. Extinction

A small but finite amount of an incident beam is absorbed as it passes through a plane. During a Bragg reflection, successive planes will continue to absorb and reflect portions of the incident beam. In addition, the reflected beam can then be reflected as it hits the underside of planes above it. This has the effect of reducing the intensity of the beam, and is referred to extinction. It is usually a concern for the lower angle reflections. [Ref. 45,p.139]

b. Atomic scattering factor and dispersion effects.

X-ray diffraction theory is based on incident waves being diffracted at a point source, namely the electron. The atomic scattering factor is defined as the ratio of the amplitude of a scattered by an atom at rest to the amplitude scattered by a single electron, and is usually given the symbol f_0. The atomic scattering factor has a value equal to the atomic number of the atom at θ equal to zero, but decreases with an increase in $(\sin\theta)/\lambda$ rather quickly. This factor takes into account the spatial distributions of the electrons for a given atom. In so doing, it assumes that the electrons are free electrons, neglecting the electronic binding energy between electrons. As long as the electronic binding energy is small compared to the energy of the X-ray photon, the scattering power of the electron will be the same as that for a free electron. However,

this scattering power may indeed be different from that of a free electron, and to account for this situation, f_0 is usually modified as follows:

$$f = f_0 + \Delta f' + i\Delta f'' \tag{3}$$

These corrections are known as the real and imaginary dispersion corrections, and are dependent on both the wavelength of radiation used and on the Bragg angle θ. For CuK_α X-rays, the excitation used in the present work, these factors are zero for lithium atoms, and negligibie for aluminum atoms [Ref. 46].

c. Structure Factor

Since very few materials have single atoms at the lattice points, the crystal structure usually consists of groups of atoms repeating a regular sequence throughout the material. To determine the intensity for a given structure, the atomic scattering factors for the individual atoms must be summed over the entire structure. This sum is the overall structure factor, F, and is defined as the ratio of the amplitude scattered by a plane (hkl) relative to the amplitude scattered by a single electron. An expression for F is:

$$F(hkl) = \sum_N f_N e^{i\phi_N} \tag{4}$$

f_N represents the atomic scattering value of the N^{th} type of atom in the cell, and ϕ_N being the phase factor. The intensity of a diffracting plane is proportional to $|F|^2$.

d. Multiplicity

The multiplicity factor arises from the fact the incident beam may be reflected from several planes, thus increasing the intensity. For powder diffraction techniques, this factor depends on the symmetry of the material, and all planes with the same interplanar spacing will reflect at the same angle θ. It is clear from the equation for d, that all permutations of a given plane (hkl) will have the same value of d.

e. Preferred orientation

Many metals tend to orient preferentially in certain directions, usually due to cold or hot working. This is described as texture, and often can result in a nonuniform distribution of crystallites. Since XRD is based on the random orientation of crystallites, the texture of a material may reduce the expected intensity in XRD.

f. Finite particle size

If precipitates form in the matrix and they are extremely small, they will tend to scatter the diffracted waves, thus reducing the height of the diffraction peak. The diffraction profile is now broadened out over a much larger range of θ, as the Bragg condition will now be met over this larger range.

g. Temperature

Since the motion of atoms is temperature dependent, it is understandable that temperature will affect the locations of the atoms and electrons in a material. This will in turn affect the observed intensities during XRD. The temperature factor is expressed as:

$$e^{-M} \tag{5}$$

This has the effect of reducing the observed intensities, especially at high angles. In this study, the ratio of intensities will be used, therefore the temperature effect will effectively be close to unity, and can be neglected [Ref. 45, p.146].

h. Lorentz-Polarization factor

This is really a combined factor. The polarization factor arises because the radiation is considered unpolarized, when in actuality it is polarized. The amount of polarization depends on the angle of diffraction. The Lorentz factor also is dependent on θ and takes into account the non-monochromatic nature of the radiation and the divergence of the beam. An expression for the Lorentz-polarization factor is:

$$\phi = \frac{1 + \cos^2 2\theta}{\sin^2\theta \cos\theta} \tag{6}$$

2. Intensity of a Diffracted Wave.

As noted above, the intensity is proportional to the square of the structure factor. By taking into account the various factors, an expression for the intensity is:

$$I^{(hkl)} = Kp\phi^{(hkl)}[F^{(hkl)}]^2 \tag{7}$$

K is a constant of proportionality, p is the multiplicity factor, and ϕ is the Lorentz-polarization factor. The temperature factor is usually included inside the structure factor F.

3. Particle Size Determination

A number of analysis methods can be used to interpret XRD data in order to determine crystallite size. Among these are the iterative folding technique and the Fourier-Transform method. Another method is to use the Scherrer equation:

$$L = \frac{K\lambda}{\beta \cos\theta} \tag{8}$$

Here, L is the particle diameter in Å, β is the pure diffraction profile expressed in radians, K is a constant, and λ and θ are as before. In order to solve for L, the pure diffraction profile must be determined. If a Gaussian line shape is assumed, the pure diffraction profile can be determined from:

$$B^2 = b^2 + \beta^2 \tag{9}$$

where B is the experimentally determined breadth of the diffraction peak, and b is the instrumental and physical strain factor.

There are three simple methods for obtaining B. These are the full-width at half-maximum, the integral breadth (area divided by height), and the variance method. If the physical strain is assumed to be zero, which is reasonable for Al-Li alloys given the small misfit strain, the instrumental factor, b, can be determined by analyzing a quartz standard which should produce no broadening. This now allows for the calculation of L, the particle diameter.

4. Volume Fraction Determination

The volume fraction of δ' can be determined by comparing the intensities of two separate diffraction peaks. For an arbitrary $L1_2$ type alloy of composition B_3A (i.e. δ'), A atoms will occupy a sites and vice versa if the alloy is ordered and at stoichiometric composition (If off-stoichiometric, atoms and sites could be interchanged). The structure factors for this situation are given as [Ref. 47]:

$$F_F^{(hkl)} = \bar{f}\left[3e^{(-M_B)} + e^{(-M_A)}\right] + .75\Delta f S\left[e^{(-M_B)} - e^{(-M_A)}\right] \tag{10}$$

$$F_S^{(hkl)} = \bar{f}\left[e^{(-M_B)} - e^{(-M_A)}\right] + .25\Delta f S\left[3e^{(-M_A)} + e^{(-M_B)}\right] \tag{11}$$

In the previous expressions:

$F_F^{(hkl)} = fundamental\ structure\ factor\ of\ \alpha$ or δ'

$F_S^{\delta'} = superlattice\ structure\ of\ \delta'$

$\bar{f} = m_A f_A + m_B f_B$

$\Delta f = f_B - f_A$

$M_{a\ or\ b} = temperature\ factor\ of\ atom\ A\ or\ B$

$S = long\ range\ order\ parameter$

In the above expressions, $f_{A\ or\ B}$ are the atomic scattering factors of A or B atoms, and $m_{A\ or\ B}$ are the atomic mass fractions of the appropriate atoms. The long range order parameter S must satisfy $0 \le S \le S_{max}$ where $S_{max} = (4/3)m_B$ $(for\ m_A \ge 0.25)$, and $S_{max} = 4m_A$ $(for\ m_A \le .25)$

Assuming $M_a = M_b = M$, for a B rich alloy, equations (10) and (11) reduce to:

$$F_F^{\alpha\ or\ \delta'} = 4(m_A^{\alpha\ or\ \delta'} f_A + m_B^{\alpha\ or\ \delta'} f_B)\exp(-M) \tag{12}$$

$$F_S^{\delta'} = S_{max}(f_B - f_A)\exp(-M) \tag{13}$$

By defining V_f as the volume fraction of δ', and noting that X-ray intensities are proportional to volume fraction, the overall structure factors, for the two phase alloy, can be written as:

$$F_S^2 = V_f(F_S^{\delta'})^2 \tag{14}$$

$$F_F^2 = (1 - V_f)(F_F^{\alpha})^2 + V_f(F_F^{\delta'})^2 \tag{15}$$

Now, by taking the ratio of the 100 and 200 intensities, from equation 7, and using equations 14 and 15 above, the volume fraction can be determined from:

$$\frac{I_{100}}{I_{200}} = \frac{\phi^{100}}{\phi^{200}}\left[\frac{F_{S,100}}{F_{F,200}}\right]^2 \tag{16}$$

$I_{100\ or\ 200}$ = Measured experimental intensity data.

$\phi^{100\ or\ 200}$ = Lorentz-polarization factors.

D. SCOPE OF PRESENT WORK

Many studies have been done on the δ' growth and aging characteristics. Most of the recent studies have utilized TEM, which has an extremely small sampling size. In previous work here at the Naval Postgraduate School, Whitman [Ref. 2] has shown that particle size can be effectively followed during growth by XRD. This study is a continuation of that work for a different alloy. Also, to the best of the authors knowledge, powder samples for the as-quenched condition have not been prepared and analyzed. Since the powder sample should provide more randomly oriented particles, it is believed that this could provide better intensity data for the diffraction peaks. This will allow for the quantitative study of the size of precipitates and the volume fractions present, which may confirm the order/disorder segregation during the initial aging period. The objectives of this study therefore are as follows:

- To verify the method of Whitman for particle growth determination by XRD.
- To prepare a powder sample for the as-quenched condition and compare results to the as-quenched flat plate results.
- To conduct an aging sequence on the powder to investigate the early aging characteristics of this alloy and to determine the effectiveness of heat treating the powder.
- To do a quantitative study of the volume fractions present after quenching and during the early aging period.

III. EXPERIMENTAL

A. SAMPLE PREPARATION

An as-cast, Al-4.1wt.%Li binary alloy, stock number 608739-A, was obtained from ALCOA.

1. Flat Plate Samples

From the ingot, plates measuring 1.0 by 0.75 by 0.125 inches were cut and then sanded down to the exact shape of the speciman holder (dimensions) for XRD. In order to minimize the effects of strain induced by polishing, the top surfaces were polished down to one micron diamond paste prior to heat treatment. The heat treatment was conducted under argon to reduce any lithium loss at high temperature as has been previously reported [Ref.48]. The samples were heat treated at 540°C for 25 minutes, followed by an ice-brine quench. All falt plate samples were placed in a freezer immediately after quenching and kept there until needed. This was necessary to avoid any room temperature aging.

2. Powder Samples

Powder was made by carefully filing a number of the flat plate samples in the as-quenched condition. Care had to be taken to avoid locally overheating the area of filing, which could induce premature aging, and to avoid inducing to much strain into the sample. To minimize these problems, the filing was conducted by submerging the sample into liquid nitrogen for approximately 1 - 2 minutes, removed and filed for about 30 seconds, and then the process repeated. This process kept the sample extremely cold and brittle, thus minimizing any heating and cold work due to filing. This was continued until enough filings were obtained. The filings were then passed through a U.S. Standard #325 sieve mesh (44 microns) to collect the powder. The powder was also placed in the freezer until needed.

B. X-RAY DIFFRACTION

A Phillips XRG 3100 X-ray generator with a copper target of wavelength 1.5405Å, and a Norelco Data Control and Processor was used for XRD. A power setting of 30kV and 35mA was used, along with a scan rate of 1 degree every 4 minutes, for all data.

1. Flat Plate Samples

Flat Plate Samples were mounted directly into the holder. Samples were marked so as to ensure a constant orientation in the holder. After heat treatment, a final 3 and

1 micron diamond polish was done prior to mo' ing. Care was taken to avoid excess pressure that might induce strain and or heat. A 30 second etch with Keller's reagent ($1\%HF, 1.5\%HCl, 2.5\%HNO_3, 95\%H_2O$) completed the flat plate preparation.

2. Powder Samples

Powder samples were mounted by mixing the powder with Acetone. Powder was poured into the holder, then lightly wetted with Acetone. This was repeated until enough powder over filled the reservoir. The top surface was then leveled by using a razor blade to remove excess powder. A final layer of Acetone was used to settle and wash away any residual powder on the holder. The Acetone mixture provided an excellent bonding of the powder and no powder was observed to displace from the holder.

C. HEAT TREATMENT

1. Flat Plate Samples

The flat plate samples were heat treated by suspended them in boiling ethylene glycol, which has a boiling temperature of 200°C. This was done to provide an oxygen and moisture free environment so as to prevent lithium loss. Heat treatments were conducted for times varying from 15 seconds to 176 hours. Samples were quenched in room temperature water after heat treatment.

2. Powder Samples

In order to age the powder, the powder was folded into a Whatman #40 filter paper, weighted down with an alligator clip, and dropped into the boiling ethylene glycol. It was also quenched in room temperature water. To recover the powder, acetone was used to wash the powder off of the filter paper. A series of washes with acetone allowed the powder to be cleaned of the ethylene glycol and then mounted directly into the holder after the final wash as described above. Powder samples were aged for periods up to one hour.

IV. RESULTS AND DISCUSSION

A. DATA REDUCTION

1. Particle Size

In order to use the Scherrer equation (eqn. 8), the pure diffraction profile β must be determined from equation 9. Using the integral breadth method, the measured breadth B can be calculated as follows:

$$B(radians) = \left[\frac{Area(in.^2)}{Height(in.)} \right] \left[Chartspeed\left(\frac{degrees}{inches} \right) \right] \left[\frac{2\pi(radians)}{360(degrees)} \right] \quad (17)$$

The height of the peak is measured directly from the output after taking out the background. The area under the diffraction profile was determined by cutting out the profile and then weighing the paper. The standard mean weight per square inch of paper was previously determined as 2.67435×10^{-2} grams per square inch, with a standard deviation of 4.134×10^{-4}. As noted earlier, due to the small misfit strain between δ' and the α matrix, b depends only on the broadening due to the instrumentation. A quartz standard was analyzed to determine b. Values for b as a function of θ are contained in Appendix C. The value of the constant K was 1.075, based on the spherical morphology of the δ' precipitates [Ref. 45, p.685]. The characteristic x-ray wavelength was 1.5405Å.

2. Volume Fraction

The intensity of the diffraction peaks, in counts, was calculated as follows:

$$Intensity\ (counts) = \left[\frac{Area(in.^2)}{chartspeed\left(\frac{in.}{sec.} \right)} \right] \left[\frac{FullScaleIntensity\left(\frac{counts}{seconds} \right)}{verticalscale(inches)} \right] \quad (18)$$

To solve equation 16 for the volume fraction of δ', the Lorentz-polarization factors, mass fractions, long range ordering parameter, and atomic scattering factors had to be determined. Lorentz-polarization factors were calculated from equation 6. S was assumed equal to $4m_A$.

To determine the atomic scattering factors for the aluminum and lithium atoms, the following summation was used.

$$f = \sum_{i=1}^{4} a_i \exp\left[-b_i \left(\sin^2 \frac{\theta}{\lambda^2} \right) \right] + C \qquad (19)$$

The values of a_i, b_i, and C were obtained from [Ref. 45, p.869]. Values for the atomic scattering factors were calculated as:

$$f_{Al}^{100} = 10.6442 \qquad f_{Li}^{100} = 2.0422$$

$$f_{Al}^{200} = 8.5077 \qquad f_{Li}^{200} = 1.6314$$

$$f_{Al}^{110} = 9.5776 \qquad f_{Li}^{110} = 1.8128$$

$$f_{Al}^{220} = 7.3143 \qquad f_{Li}^{220} = 1.3940$$

The atom fractions, assuming α and δ' are ordered and of the same composition, are:

$$m_{Al}^{\alpha} = m_{Al}^{\delta'} = 0.8575$$

$$m_{Li}^{\alpha} = m_{Li}^{\delta'} = 0.1425$$

The volume fraction of δ' can now be calculated from equation 16.

B. AS-QUENCHED RESULTS

Intensity, integral breadth, and particle size results of all heat treatments for both plate and powder samples are tabulated in Appendices A and B, respectively. Table 2 summarizes the calculated values of particle size, volume fraction, long range order and intensities for the as-quenched condition for the plate and powder samples.

Table 2. COMPARISON OF AS-QUENCHED RESULTS (BASED ON I_{100}/I_{200})

	Plate Sample	Powder Sample
δ' particle size (diameter)	32Å	42Å
Volume Fraction (δ')	0.53	0.77
Long range order parameter	0.415	0.500
$I_{100}(counts)$	5,391	16,057
$I_{200}(counts)$	80,541	165,685
$I_{110}(counts)$	Not detected	9,259
$I_{220}(counts)$	Not measured	127,707

The plate sample showed a very broadened 100 δ' peak. Also present was the 111 δ peak. The 110 δ' peak was not present in the as-quenched condition. The 100 δ' peak had a weak intensity, but was measurable. The determination of the background and the extreme broadening associated with this peak made accurate results difficult. However, the as-quenched particle size is in good agreement with that of other investigators.

The powder sample as-quenched diffraction pattern for the 2θ range of 16 to 45 degrees is shown in Figure 8 on page 27. Clearly visible are both the 100 and 110 superlattice reflections associated with δ', and also the 111 and 220 peaks correlating to the presence of δ. The intensity of the 100 peak for the powder sample is clearly larger than the intensity for the plate sample, as can be seen from Table 2. The increase in intensity for the powder sample, coupled with the presence of both the 110 δ' peak and the 220 δ peak, clearly indicate that there are pronounced preferred orientation effects in the plate sample.

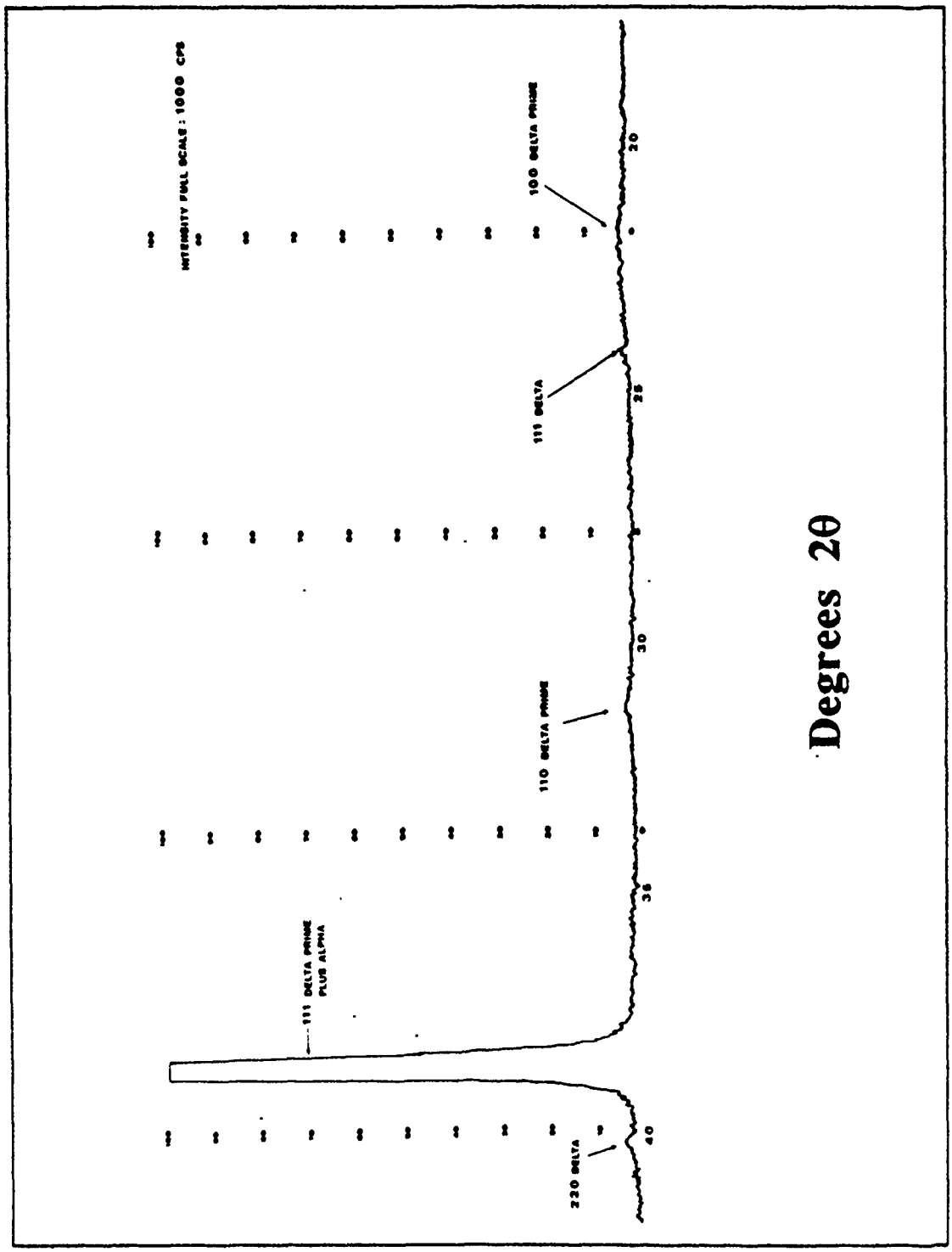

Figure 8. XRD Output for Powder Sample (As-quenched)

Table 3 on page 28 shows the intensities and particle sizes for the powder sample in the as-quenched condition. Due to the presence of both the 100 and 110 δ' peaks, it was possible to calculate the δ' particle size from both diffraction profiles. This now gives an average δ' particle size of 53Å, which is somewhat higher than the plate value. The major concern with the powder sample was that premature aging might be introduced, leading to an increase size of the ordered regions. While it may appear that perhaps aging did occur, a couple of points must be brought out. Although not clear from Figure 8 on page 27, there was overlap between the diffraction peaks.

Table 3. AS-QUENCHED INTENSITY AND PARTICLE SIZE OF POWDER SAMPLE

Diffraction Peak	Intensity (counts)	Particle Size (Å)
100 (δ')	16,057	42.25
111 (δ)	715.7	774
110 (δ')	9,259	64.2
111	296,707	368
220 (δ)	1,864	357
200	165,685	330
220	127,707	256
311	158,259	239
222	45,364	247

The 100 and 110 peaks had slight overlap, but this was not considered a major source of error. However, the 110 superlattice and 111 fundamental had extensive overlap, making the accurate determination of the background extremely difficult for these peaks. This resulted in an underestimation of the intensity and area under both these profiles, leading to a higher prediction of the particle size based on the Scherrer equation. Therefore, the δ' particle size based on the 110 peak is probably high, and the 100 result can be taken as the more accurate value. This is further emphasized by noting a similar result for the particle size predicted by the fundamental peaks. As can be seen from Table 3, the 111 fundamental predicts the highest particle size. This again is due to the errors in the determination of the area and intensity of this peak. Now, when considering whether the powder sample had been prematurely aged, a comparison of the plate value of 32Å to the powder value of 42Å shows there is not a great difference, especially

when considering the experimental errors for both samples, and the preferred orientation effects of the plate. Hence, it is safe to say that the powder preparation did not result in any premature aging and gives a truer representation of the crystal structure.

The value of 77% ordered regions and a long range order parameter of 0.50 indicate a highly ordered structure in the as-quenched condition. In fact, the maximum order for this alloy is predicted by theory to be 0.57, so indeed it is very much ordered. By calculating the size of the disordered regions, which occupy the remaining 23% of the alloy, an average particle size would be 1070Å. This high degree of order fits the theoretical model of Khachaturyan. Recall that this model predicts a congruent ordering transformation prior to the decomposition to the two-phase mixture. Recent (May,1990) work by Shaiu et al. using SAXS have also shown that a supersaturated solid solution phase appears to undergo a congruent ordering prior to decomposition [Ref. 49]. They also found no evidence for a metastable miscibility gap, as predicted by Sigli and Sanchez.

Previous work by Fox has resulted in the HREM micrograph shown in Figure 9 on page 30. This micrograph clearly shows ordered regions of a size approximately 50Å, although their shape is difficult to determine. Based on the observations and results of the as-quenched powder sample, and coupled with the theoretical model of Khachaturyan and the work of other investigators, it appears that the as-quenched microstructure of this alloy consists of a two-phase region in which the majority is ordered particles with an average size of 42Å surrounded by a sea of disordered matrix for this alloy.

C. AGING CHARACTERISTICS.

For the plate sample, the growth of the δ'particles followed Ostwald ripening. The radius of the δ' particles is plotted against aging time in Figure 10 on page 31. A plot of the radius cubed against aging time is shown in Figure 11 on page 32. These two plots are typical of Ostwald coarsening kinetics, and confirm previous investigations.

During the aging of the plate sample, a rapid decrease in the intensity of the 200 fundamental peak was observed. This resulted in a sharp increase in the ratio of I_{100}/I_{200}. Figure 12 on page 33 shows this ratio increase, which occurred during the first minute of aging. This might be an effect of the preferred orientation in the plate that causes this peak to lose proper orientation to cause diffraction. This loss could also be explained if there was an initial coherency loss between the matrix and the precipitate. The results of Radmilovic et al. indicate that the initial precipitates are coherent, based on TEM observations [Ref. 26]. If, during the early stages of aging, as the ordered

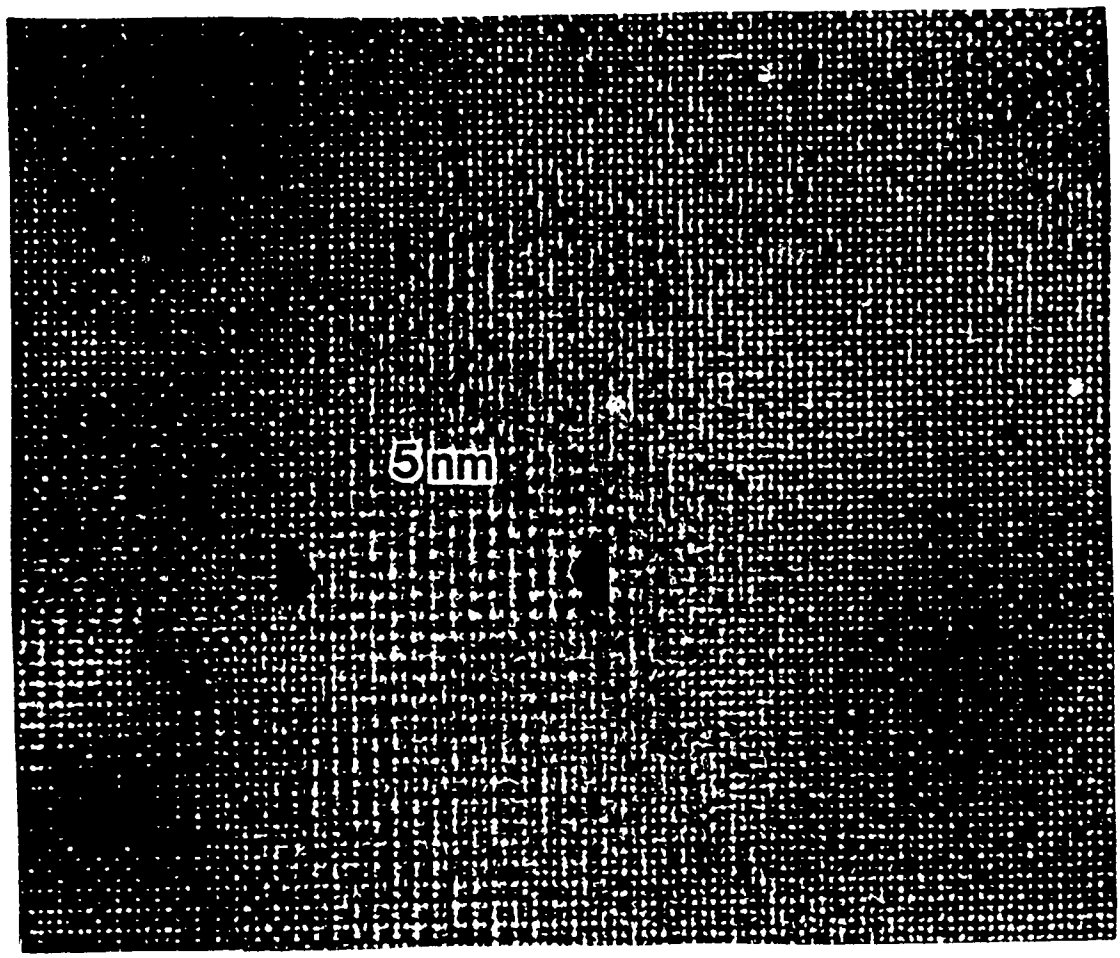

Figure 9. HREM Micrograph of an As Quenched Al-Li Alloy: Beam direction, B = [100]. A 50Å(5nm.) ordered area is marked. This is the developing δ' particle. (Micrograph courtesy A.G. Fox)

regions develop into δ', there is a temporary loss of coherency, the result could be a rotation of the matrix in the plate away from the proper Bragg angle enough to have the contributions of the matrix to the fundamental peak be eliminated. This would mean the only contributions to the 200 peak were the δ' particles, as they are for the superlattice peak. This would account for the reduction in intensity of the fundamental.

The powder sample aging sequence also gave a fluctuation in the intensity ratio between the 100 and 200 peaks, but not nearly as severe. Figure 13 on page 35 shows the variation of the intensity ratio. The powder sample has a similar rise in the ratio, followed by a gradual decrease. Figure 14 on page 36 shows the intensity ratio observed between the 110 and 220 peaks. This ratio also shows a minor inflection. These results

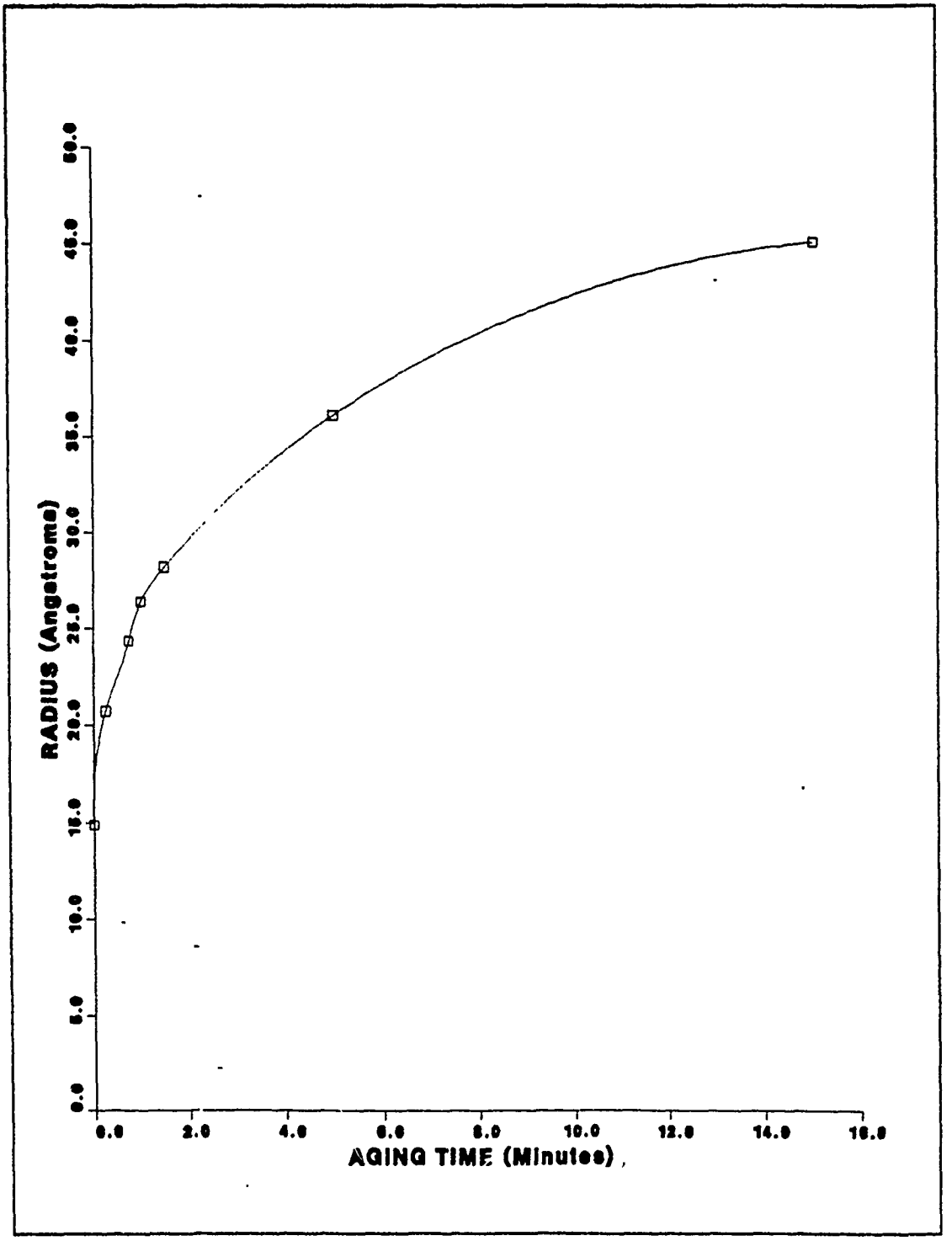

Figure 10. δ' Radius versus Aging Time (Plate Sample)

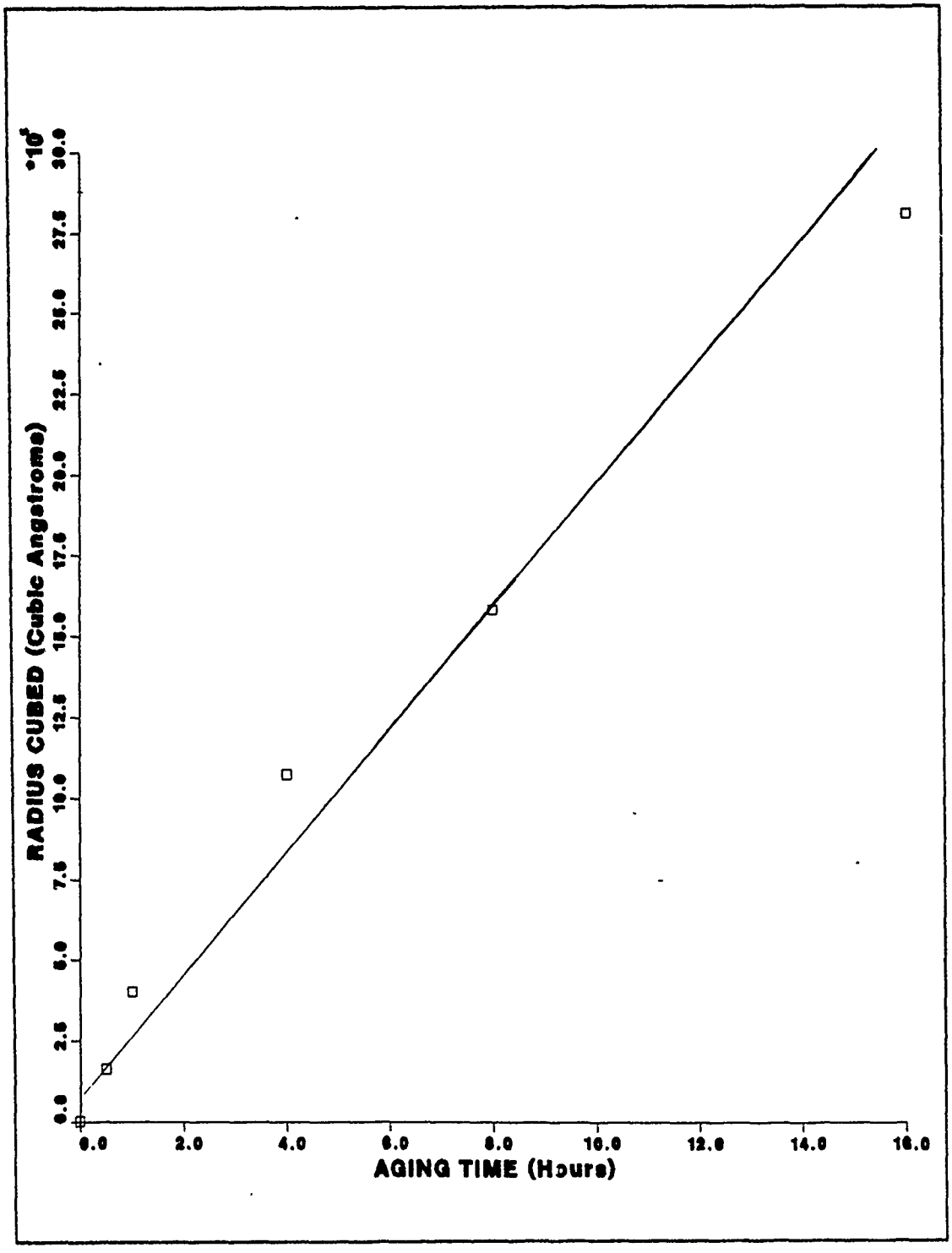

Figure 11. δ' Radius Cubed versus Aging Time (Plate Sample)

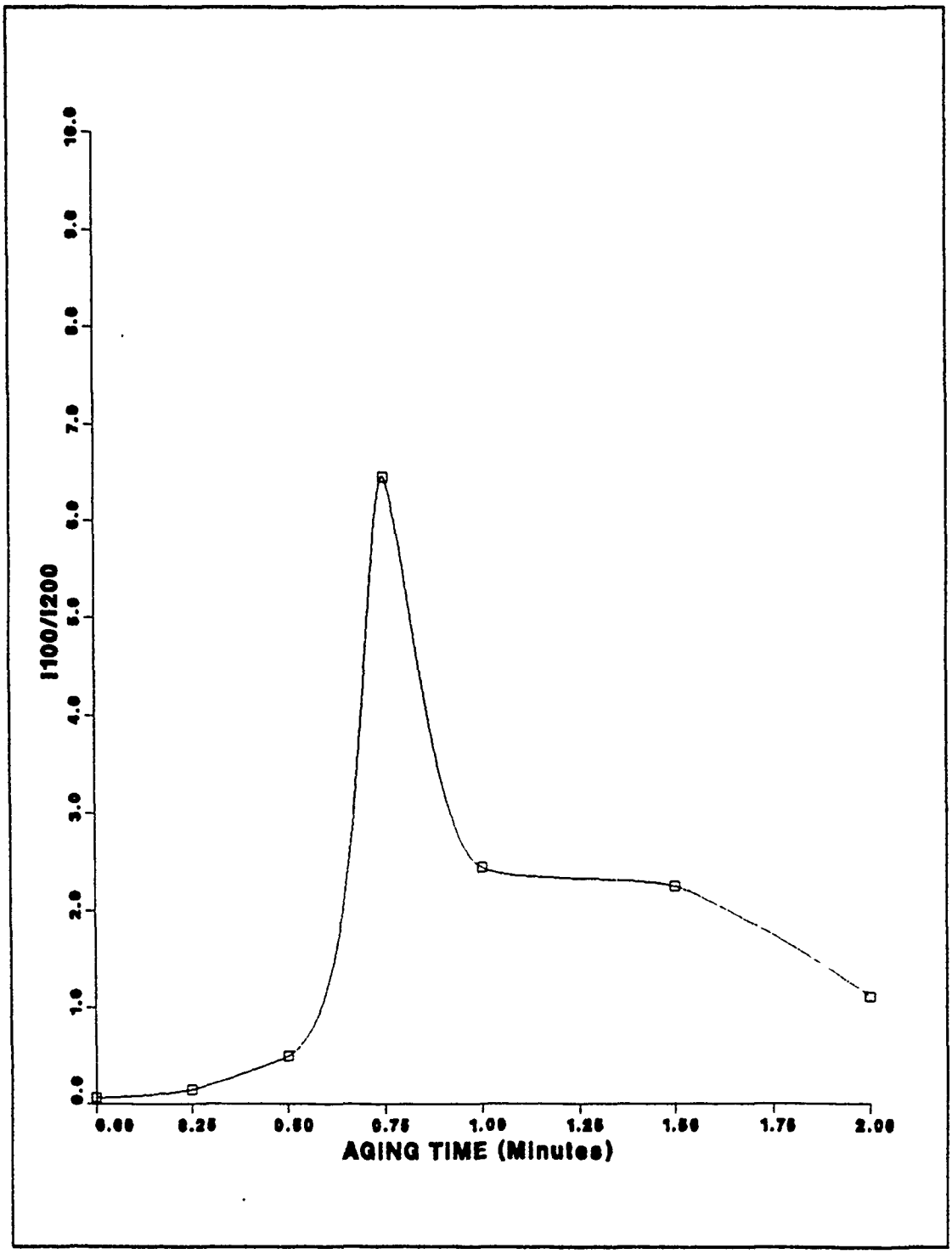

Figure 12. I_{100}/I_{200} versus Aging Time (Plate Sample)

tend to indicate that perhaps there is some early aging characteristics happening that are not fully understood. However, it should be noted that this is a first attempt of a heat treatment procedure for the powder, and may have to be researched further. There is the possibility that lithium losses during the heat treatment of the powder have invalidated the aging results of this sample due to the large surface area to volume ratio of the powder as compared to the plate. This will allow for a greater opportunity of lithium loss in the powder sample.

This can be further deduced for Figure 15 on page 37 that shows the δ'radius growth with aging time. There is a definite inflection in this graph at the early stages of aging, also indicating that perhaps some unexplained occurrence is happening. But once again, this may be due to problems associated with the experiment, especially lithium losses which would certainly lead to lower values for the particle size of δ' The graph does almost flatten out during the 2-15 minute range for the 110 data. There is also the possibility that the heat treatment is not uniform, thus resulting in the drop of average particle size. This phenomenon has been noticed before by Spooner et al., but at a much longer aging time. They noticed a decrease during the 5-10 hour aging period. They proposed that perhaps a spinodal decomposition in the matrix with fast coarsening was followed by the nucleation of more stable δ' at a smaller size, thus reducing the average particle size. [Ref. 31, p.333]

The presence of the δ phase was noted throughout this investigation. Many investigators have reported that they have avoided the formation of the δ phase during their experiments. Due to this alloy being close to the solid solubility of lithium in aluminum, and given the uncertainties in the phase diagram, there is the possibility that this alloy was not solution heat treated at a high enough temperature. However, the results of Whitman clearly indicated the presence of δ after quenching from the solid solution [Ref. 2]. The formation and presence of δ is considered detrimental to the mechanical properties of the alloy. For the present study, a volume fraction calculation indicates less than 0.1% of the δ phase is present in the as-quenched state. Therefore, it is reasonable to assume that the presence of δ did not affect the results generated for the δ' phase in the as-quenched state. However, for the aging sequence in the powder, the δ phase did grow (see Appendices A and B). This of course requires lithium, and therefore is another possible source of lithium loss to the δ' in addition to the previously mentioned sources above.

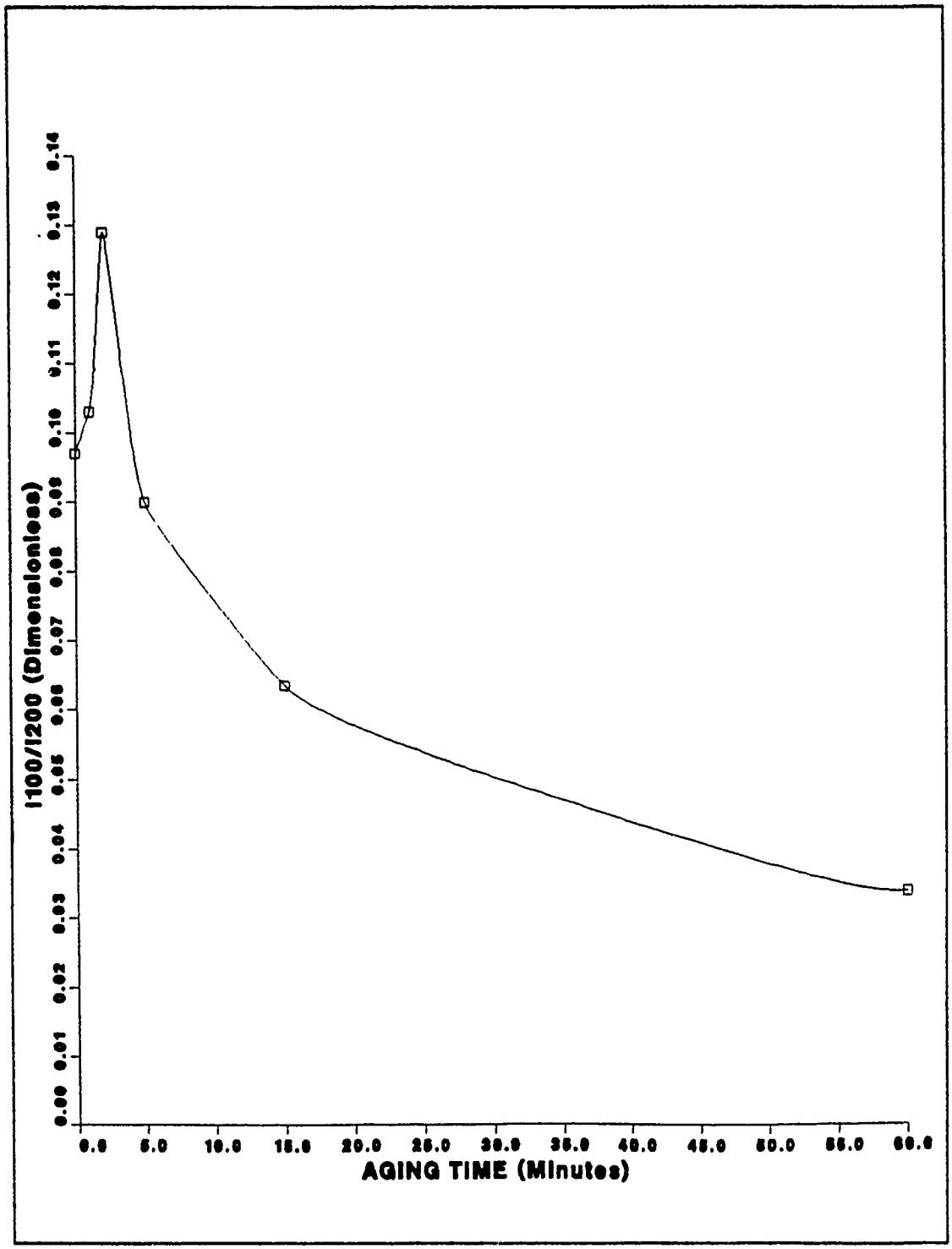

Figure 13. I_{100}/I_{200} versus Aging Time (Powder Sample)

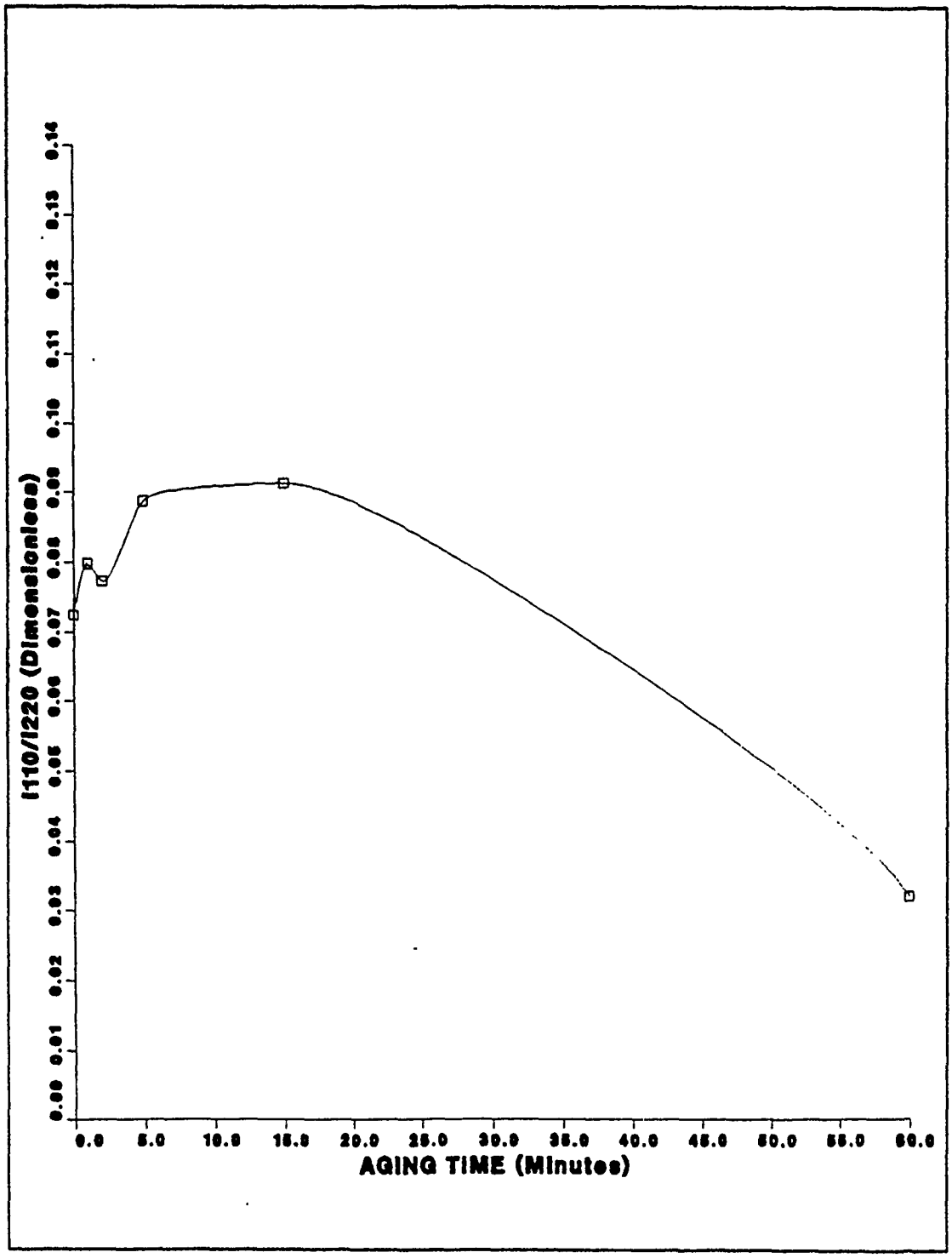

Figure 14. I_{110}/I_{220} versus Aging Time (Powder Sample)

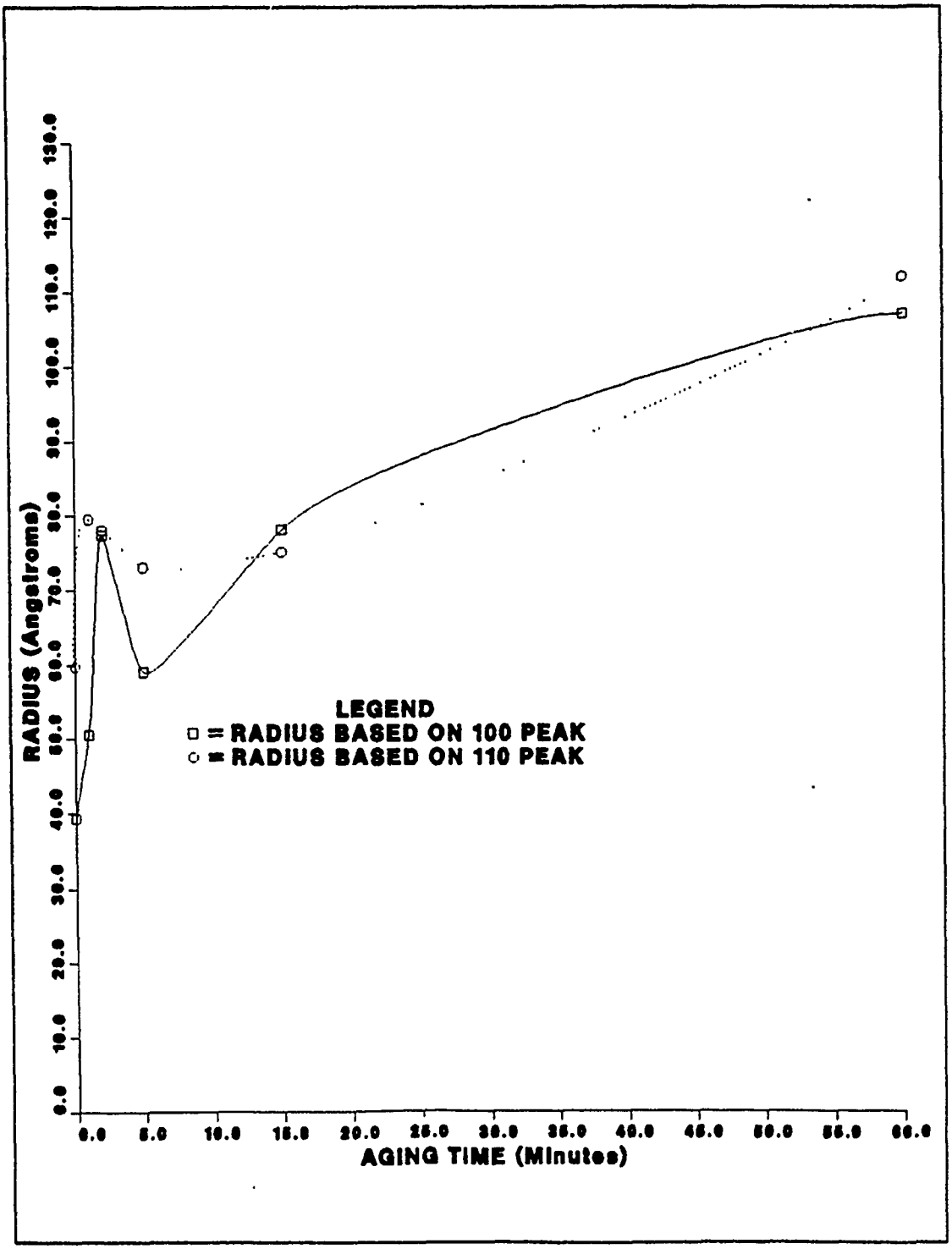

Figure 15. Delta Prime Radius versus Aging Time (Powder Sample)

D. ERROR ANALYSIS

The major source of error for an XRD experiment is in the exact determination of the profile and the background. Since the error in profile is directly proportional to the particle size error, the error in profile determination will give the particle size error. The following fractional error expression has been used [Ref. 45 , pp.361-364]:

$$\frac{d\beta}{\beta} = \frac{\sqrt{N_e}}{N_e} + \frac{dh_e}{h_e} + \frac{\sqrt{N_s}}{N_s} + \frac{dh_s}{h_s}$$

β = Pure profile breadth
N_e = No. of counts under experimental peak
h_e = Height of experimental peak
N_s = No. of counts under quartz standard peak
h_s = Height of quartz standard peak
dh = .1in. (accuracy of measurement)

Table 4 summarizes the percent error determined for the as- quenched results of particle size for both the plate and powder samples. As can be seen from Table 4, the powder sample generally had slightly less of a fractional error, once again indicating the preferred orientation effects of the plate and the overall success of the powder experiment. Appendices A and B have complete errors contained in them for all aging times.

Table 4. PERCENT ERROR IN PARTICLE SIZE BASED ON I_{100}

Heat Treatment Time (minutes)	Percent error (plate sample)	Percent error (powder sample)
As-quenched	17.3	6.8
1	11.4	6.4
2	10.5	6.0
5	9.8	5.8
15	8.1	6.3
60	7.4	8.4

V. CONCLUSIONS

This investigation studied the early aging characteristics of an Al-Li alloy by utilizing both plate and powder samples. The plate samples clearly indicated a preferred orientation effect, thus limiting their effectiveness in this study. The powder sample gave excellent results for the as-quenched condition. From the as-quenched powder sample, it was possible to model the as-quenched microstructure as a two-phase region consisting of 77% ordered regions with an average size of 42Å surrounded by a disordered matrix. This model fits other experimental data as well as the theoretical model of Khachaturyan. The aging experiment on the powder did not lead to any conclusive results, and indicated that the technique attempted in this experiment may not be valid. This was most probably due to lithium losses incurred during the heat treatment, both to the atmosphere and to the growth of the δ phase, which was observed throughout this study. The presence of the Al-Li δ phase needs to be addressed by further study, as does the aging procedure for the powder.

VI. RECOMMENDATIONS

The following recommendations are given for additional research into Al-Li alloys:

- The powder method gave excellent results for the as-quenched state, but should be duplicated to verify the making of the powder sample.

- The heat treatment of the powder appears to limit the growth of the δ'. A better sequence might be to heat treat the plates and make the powder sample after each heat treatment. Although this would be very time consuming, it would probably give results similar to this studies as-quenched results, allowing for a better understanding of the initial aging characteristics.

- In order to better determine if δ is present in the as-quenched state, a higher solution heat treatment temperature should be tried for this alloy.

APPENDIX A. EXPERIMENTAL RESULTS (PLATE SAMPLE)

Table 5. EXPERIMENTAL RESULTS OF PLATE SAMPLE (0-30 MINUTES)

Heat Treatment	Peak (hkl)(phase)	Intensity (counts)	Integral Breadth (radians)	Particle Size (Å)	Percent Error in Particle Size
As Quenched	100(δ')	5391	0.0527	31.97	17.3
	200	80541	0.0020	--	--
	111(δ)	558.6	0.0026	--	--
15 sec.	100(δ')	5961	0.0378	44.52	12.5
	200	40024	0.0021	--	--
	111(δ)	664	0.0035	694.0	12.9
30 sec.	100(δ')	6461	0.0379	44.4	11.8
	200	12923	0.0022	--	--
	111(δ)	633	0.0026	--	--
45 sec.	100(δ')	5203	0.0321	52.35	20.2
	200	538.5	0.0026	--	--
	111(δ)	471	0.0020	--	--
1 min.	100(δ')	5416	0.0296	56.8	11.4
	200	2218	0.0035	--	--
	111(δ)	592.3	0.0027	--	--
1.5 min.	100(δ')	5676	0.0277	60.6	10.6
	200	2524	0.0026	--	--
	111(δ)	455.4	0.0021	--	--
2 min.	100(δ')	4871	0.0233	72.0	10.6
	200	4395	0.0036	--	--
	111(δ)	507	0.0021	--	--
5 min.	100(δ')	5070	0.0216	77.5	9.8
	200	1057	0.0034	--	--
	111(δ)	366	0.0018	--	--
15 min.	100(δ')	5584	0.0172	96.9	8.1
	200	1517	0.0099	190.4	15.5
	111(δ)	283	0.0017	--	--
30 min.	100(δ')	5607	0.0141	117.6	7.4
	200	938	0.0079	246.2	18.7
	111(δ)	294	0.0029	--	--

Table 6. EXPERIMENTAL RESULTS OF PLATE SAMPLE (1 - 172 HOURS)

Heat Treatment	Peak (hkl)(phase)	Intensity (counts)	Integral Breadth (radians)	Particle Size (Å)	Percent Error in Particle Size
1 hour	100(δ')	5066	0.0103	158.8	7.4
	200	911	0.0079	246.2	19.2
	111(δ)	294	0.0020	--	--
4 hours	100(δ')	6161	0.0072	220.2	5.5
	200	1362	0.0103	182.2	17.0
	111(δ)	249	0.0029	--	----
8 hours	100(δ')	6639	0.0062	250.7	5.1
	200	294	0.0043	598	30.0
	111(δ)	357	0.0030	--	--
16 hours	100(δ')	6215	0.0049	304	6.0
	200	1463	0.0078	250	13.9
	111(δ)	296	0.0035	--	--
32 hours	100(δ')	8153	0.0043	335	5.1
	200	2340	0.0077	254	10.6
	111(δ)	202	0.0024	--	----
172 hours	100(δ')	10444	0.0028	440	5.4
	200	2614	0.0055	393	8.8
	111(δ)	226.6	0.0031	--	--

APPENDIX B. EXPERIMENTAL RESULTS (POWDER SAMPLE)

Table 7. AS-QUENCHED DATA (POWDER SAMPLE)

Peak (hkl and phase)	Intensity (counts)	Integral Breadth (rads)	Particle Size (Å)	Percent Error in Particle Size
100(δ')	16057	0.03996	42.25	6.8
111(δ)	715.7	0.00333	774	11.9
110(δ')	9259	0.02693	64.2	10.5
111	296707	0.00558	368	3.85
220(δ)	1864	0.00575	357	8.93
200	165685	0.00624	330	6.84
220	127707	0.00856	256	5.82
311	158259	0.00993	239	4.02
222	45364	0.00996	247	5.4

Table 8. 1 MINUTE AGE RESULTS (POWDER SAMPLE)

Peak(hkl and phase)	Intensity (counts)	Integral Breadth (rads)	Particle Size (Å)	Percent Error in Particle Size
100(δ')	14477	0.0312	54.3	6.38
111(δ)	2300	0.0037	639.0	6.05
110(δ')	8773	0.0203	85.5	9.70
111	253743	0.0047	474	3.85
220(δ)	4496	0.0043	564	6.49
200	140714	0.0052	426	5.29
220	109799	0.0068	348	5.70
311	139596	0.0083	300	3.96
222	41550	0.0087	296	5.35

Table 9. 2 MINUTE AGE RESULTS (POWDER SAMPLE)

Peak (hkl and phase)	Intensity (counts)	Integral Breadth (rads)	Particle Size (Å)	Percent Error in Particle Size
100(δ')	11173	0.0205	83.2	6.1
111(δ)	3376	0.0043	490.0	5.2
110(δ')	9955	0.0207	83.8	9.3
111	293670	0.0054	386	3.8
220(δ)	5510	0.0046	499	6.0
200	86826	0.0030	----	----
220	128644	0.0076	299	5.6
311	159876	0.0085	294	3.8
222	22090	0.0041	288	5.4

Table 10. 5 MINUTE AGE RESULTS (POWDER SAMPLE)

Peak (hkl and phase)	Intensity (counts)	Integral Breadth (rads)	Particle Size (Å)	Percent Error in Particle Size
100(δ')	15584	0.0270	63.0	5.8
111(δ)	3482	0.0035	685.0	4.9
110(δ')	11162	0.0222	78.0	9.1
111	298726	0.0044	535	3.6
220(δ)	5968	0.0038	745	5.4
200	174546	0.0049	569.0	6.2
220	125772	0.0065	369	5.4
311	158528	0.0075	346	3.6
222	45861	0.0073	379	5.1

Table 11. 15 MINUTE AGE RESULTS (POWDER SAMPLE)

Peak (hkl and phase)	Intensity (counts)	Integral Breadth (rads)	Particle Size (Å)	Percent Error in Particle Size
100(δ')	10282	0.0208	83.8	6.3
111(δ)	3724	0.0037	632.0	4.8
110(δ')	10282	0.0216	80.4	9.3
111	290089	0.0045	514	3.6
220(δ)	5912	0.0035	923	7.8
200	162207	0.0049	462.0	6.4
220	112670	0.0059	433	5.4
311	150137	0.0075	346	3.7
222	41180	0.0070	406	5.1

Table 12. 1 HOUR AGE RESULTS (POWDER SAMPLE)

Peak (hkl and phase)	Intensity (counts)	Integral Breadth (rads)	Particle Size (Å)	Percent Error in Particle Size
100(δ')	4658	0.0150	115	8.4
111(δ)	3336	0.0041	516	5.2
110(δ')	3444	0.012	149	11.8
111	249256	0.0047	465	3.9
220(δ)	14751	0.0041	605	5.1
200	138538	0.0050	444	6.8
220	107600	0.0063	389	5.6
311	136496	0.0075	350	3.8
222	40922	0.0075	365	5.2

APPENDIX C. INSTRUMENTAL BROADENING (BASED ON A QUARTZ STANDARD)

Table 13. QUARTZ STANDARD DATA

Position (2θ)	Intensity (counts)	Integral Breadth (radians)	Total Fractional Error
20.98	20057	0.002745	0.02589
26.6	114642	0.00247	0.01777
31.1	3085	0.0033	0.05436
36.6	11958	0.0028	0.02547
39.6	12766	0.0028	0.02377
42.5	10118	0.0031	0.03113
45.7	7247	0.0030	0.04006
50.4	29210	0.0032	0.02109
60.0	25105	0.0037	0.01644
64.2	4846	0.0032	0.03698
75.7	9614	0.0041	0.02488
83.7	6944	0.0045	0.03422

LIST OF REFERENCES

1. Glazer, J., "The strength-toughness combination of the Aluminum-Lithium Alloys 2090 and 2091 at Cryogenic Temperatures", Ph.D Thesis, Materials and Chemical Division, Lawrence Berkeley Laboratory, Univ. of Ca., Berkeley, Ca., July, 1989.

2. Whitman, C. E., "An Investigation of Delta Prime Growth in an Aluminum-lithium Alloy using X-ray Diffraction Analysis", Masters Thesis, Naval Postgraduate School, Monterey, Ca., March 1990.

3. Balmuth, E. S., and Schmidt, R., "A Perspective on the Development of Aluminum-Lithium Alloys", *Aluminum-Lithium Alloys*, Sanders, T. H. and Starke, E. A., eds., The Metallurgical Society of AIME, 1981.

4. Prichett, T. R., "Advanced Technology Aluminum Materials for Aerospace Applications", *Aluminum Technology'86*,, Sheppard, T., ed., Institute of Metals, 1986.

5. Evans, R. K., "Western World Lithium Reserves" *Al-Li Alloys III, University of Oxford, 8-11 July 1985*, Gregson, P.J., Harrison, S.J., and Peel, C.J.,eds.,Institute of Metals, London, 1986.

6. Peel, C. J., and others, "The Development and Application of Improved Al-Li Alloys" *Aluminum-Lithium Alloys II*, Sanders, T. H. and Starke, E. A., eds., The Metallurgical Society of AIME, 1984.

7. Little, D., "Overview", *Al-Li Alloys III, University of Oxford, 8-11 July 1985*, Gregson, P.J., Harrison, S.J., and Peel, C.J.,eds.,Institute of Metals, London, 1986.

8. Wadsworth, J. "Superplasticity Behavior of Al-Li Alloys", *Aluminum-Lithium Alloys II*, Sanders, T. H. and Starke, E. A., eds., The Metallurgical Society of AIME, 1984.

9. Averill, W. A., Olson, D. L., Matlock, D. K., and Edwards, G. R., "Lithium Reactivity and Containment", *Aluminum-Lithium Alloys*, Sanders, T. H. and Starke, E. A., eds., The Metallurgical Society of AIME, 1981.

10. Gregson, P. J. and Flower, H. M., "δ' Precipitation in Al-Li-Mg-Cu-Zr Alloys", *J. Mat. Sci. Letters*, 3, pp.829-834, 1984.

11. Makin, P. L. and Ralph, B., "On the Ageing of an Aluminum-Lithium-Zirconium Alloy", *J. Mat. Sci.*, 19, pp.3835-3843, 1984.

12. Gayle, F. W. and Vandersande, B., "Phase Transformations in the Al-Li-Zr System", *Acta. Metall.*, Vol. 37, No. 4, pp. 1033-1046, 1989.

13. Roy, G., "Status of Al-Li Development at Pechiney", *Al-Li Conference, March 25-26, 1987, Los Angeles, Ca.*, Ramesh, J.,Suphal, P., and Quist, W. eds., ASM 1987.

14. Forness, S. and Heckman, E. A. W., "The Use of 8090 in the McDonell-Douglas F15 SMTD Aircraft", *Al-Li Conference, March 25-26, 1987, Los Angeles, Ca.*, Ramesh, J.,Suphal, P., and Quist, W. eds., ASM 1987.

15. Sigli, C. and Sanchez, J. M., "Calculation of Phase Equilibrium in Al-Li Alloys", *Acta. Metall.*, Vol.34, No.6, pp. 1021-1028, 1986.

16. Quist, W. E., Narayanan, G. H., and Winget, A. L., "Al-Li Alloys for Aircraft Structure-An Overview", *Aluminum-Lithium A loys II*, Sanders, T. H. and Starke, E. A., eds., The Metallurgical Society of AIME, 1984.

17. Williams, D. B., "Microstructural Characteristics of Al-Li Alloys" *Aluminum-Lithium Alloys*, Sanders, T. H. and Starke, E. A., eds., The Metallurgical Society of AIME, 1981.

18. Liu, D. R. and Williams, D. B., "Determination of the δ' Solvus Line in Al-Li Alloys by Measurement of the δ' Volume Fraction", *Scripta Metall.*, Vol. 22, pp. 1361-1365, 1988.

19. Cocco, G.,Fagherazzi, G. and Schiffini, L., "Determination of the δ' Coherent Miscibility Gap in the Al-Li System by Small-Angle *X*-Ray Scattering", *J. Appl. Cryst.*, Vol.10, pp.325-327, 1977.

20. Jha, S. C., Sanders, T. H., and Dayananda, M. A., "Grain Boundary Precipitate Free Zones in Al-Li Alloys", *Acta. Metall.*, Vol. 35, No. 2, pp. 473-482, 1987.

21. Radmilovic, V., Fox, A. G., Fisher, R. M., Thomas, G. "Lithium Depletion in Precipitate Free Zones (PFZ's) in Al-Li Base Alloys", *Scripta Met.* Vol. 23, pp. 75-79, 1989.

22. Sanders, T. H., "Al-Li-X Alloys--An Overview", *Aluminum-Lithium Alloys*, May 1980.

23. Baumann, S. F. and Williams, D. B., "Effects of Capillarity and Coherency on δ' (Al_3Li) Precipitation in Dilute Al-LI Alloys at Low Undercoolings", *Acta. Metall.*, Vol.33, No.6, pp.1069-1078, 1985.

24. Gu, B., Mahalingam, K., Liedl,G. L., and Sanders, T. H., "The Delta Prime Particle Size Distributions in a Variety of Al-Li Alloys" *Al-Li Alloys III, University of Oxford, 8-11 July 1985*, Gregson, P.J., Harrison, S.J., and Peel, C.J.,eds.,Institute of Metals, London, 1986.

25. Gu, B. P., Liedl, G.L., Kulwicki, J. H., Sanders, T. H., "Coarsening of Delta Prime Precipitates in an Al-2.8Li-0.3Mn Alloy", *Mat. Sci. Eng.*, Vol. 70, pp. 217-228, 1985.

26. Radmilovic, V., Fox, A. G. and Thomas, G., "Spinodal Decomposition of Al-Rich Al-Li Alloys", *Acta. Metall.*, Vol.37, No.9, pp.2385-2394,1989.

27. Williams, D. B., and Edington, J. W., "The Precipitation of $\delta'(Al_3Li)$ in Dilute Aluminum-Lithium Alloys", *Metal Science*, Vol.9, pp.529-532, 1975.

28. Flower, H. M., and Gregson, P. J., "Solid State Phase Transformations in Aluminum Alloys Containing Lithium", *Mat. Sci. Tech.*, 3, pp. 81-90, 1987.

29. Khachaturyan, A. G., Lindsey, T. F., and Morris, J. W., "Theoretical Investigation of the Precipitation of δ' in Al-Li", *Met. Trans. A*, Vol.19A, Feb. 1988.

30. Sato, T., Tanaka, N., and Takahashi, T., "High Resolution Lattice Images of Ordered Structures in Al-Li Alloys", *Trans. JIM*, Vol. 29, No. 1, pp. 17-25, 1988.

31. Spooner, S., Williams, D., Sung, C., "Combined Small Angle X-Ray Scattering and Transmission Electron Microscopy Studies of Al-Li Alloys", *Al-Li Alloys III, University of Oxford, 8-11 July 1985*, Gregson, P.J., Harrison, S.J., and Peel, C.J.,eds.,Institute of Metals, London, 1986.

32. Chen, S. W., Jan, C. H., Lin, J. C. and Chang, Y. A., "Phase Equilibria of the Al-Li System", *Met. Trans. A*, Vol. 20A, Nov. 1989.

33. Noble, B., Harris, S. J., and Dinsdale, K., "The elastic modulus of aluminum-lithium alloys", *J. Mat. Sci.*, 17, pp. 461-468, 1982.

34. Sanders, T. H. and Starke, E. A., "The Effects of Slip Distribution on the Monotonic and Cyclic Ductility of Al-Li Binary Alloys", *Acta. Metall.*, Vol.30, pp.927-939, 1982.

35. Fox, A. G. and Fisher, R. M., "Structure Factors and Debye Temperatures of Al-Li Solid-Solution Alloys", *Acta. Cryst.*, A43, pp.260-265, 1987.

36. Fox, A. G. and Fisher, R. M., "The Origin of the High Elastic Modulus in Al-Li Alloys", *J. Mat. Sci. Letters*, 7, pp. 301-303, 1988.

37. Noble, B. and Thompson, G. E., "Precipitation Characteristics of Aluminum-Lithium Alloys", *Met. Sci. J.*, Vol. 5, pp.114-120, 1971.

38. Furukawa, M., Miura, Y., and Nemoto, M., "Arrangement of Deformation Induced Dislocations in Aged Al-Li Alloys", *Trans. JIM*, Vol.26, No. 4, pp. 225-229,1985.

39. Noble, B., Harris, S.J., Dinsdale, K., "Yield Characteristics of Aluminum-Lithium Alloys" *Met. Sci.* Vol.16, No.9, Sept. 1982.

40. Furukawa, M., Miura, Y., and Nemoto, M., "Strengthening Mechanisms in Al-Li Alloys Containing Coherent Ordered Particles", *Trans. JIM*, Vol.26, No.4, pp. 230-235, 1985.

41. Sanders, T. H., "$\delta'(Al_3Li)$ Morphology and Its Influence on the Mechanical Behavior of Aluminum-Lithium Alloys", *International Light Metals Conference, 8th*,1987.

42. Sung,C. M., Chan, H. M., and Williams, D. B., "Quantitative Microanalysis of Li in binary Al-Li Alloys", *Al-Li Alloys III, University of Oxford, 8-11 July 1985*, Gregson, P.J., Harrison, S.J., and Peel, C.J.,eds.,Institute of Metals, London, 1986.

43. Chan, H. M., Williams, D.B., "Quantitative Analysis of Lithium in Al-Li Alloys by Ionization Energy Loss Spectroscopy", *Phil. Mag.*, Vol.52, No.5, 1019-1032, 1985.

44. Pickering, H. W., "(1) Atomistic Study of Metastable Phases in an Al-3wt.%Li-0.12%-Zr Alloy ,(2)A Preliminary Study of Al-Li Alloys using Atom-Probe Field Ion Micros copy and Transmission Electron Microscopy", *Office of Naval Research Technical Report No. N00014-84-k-0201, 2 March 1987.*

45. Klug, H. P. and Alexander, L. E., *X-Ray Diffraction Procedures*, Chapter 9, John Wiley and Sons, 1974.

46. Templeton, D. H., in *International Table for X-ray Crystallography*, Vol.III, Sect.3.3,pp.213-216, Birmingham: Kynoch Press, 1962.

47. Warren, B. E., *X-Ray Diffraction*, Addison-Wesley, 1969.

48. Burke, M., Papazian, J. M., "Elevated Temperature Oxidation of Al-Li Alloys", *Al-Li Alloys III, University of Oxford, 8-11 July 1985*, Gregson, P.J., Harrison, S.J., and Peel, C.J.,eds.,Institute of Metals, London, 1986.

49. Shaiu, B. J., Li, H. T., Lee, H. Y., and Chen, Hadyn, "Decomposition and dissolution Kinetics of δ' Precipitation in Al-Li Binary Alloys", *Met. Trans.*. Vol. 21A-No.5, pp. 1133-1141, May, 1990.

INITIAL DISTRIBUTION LIST

		No. Copies
1.	Defense Technical Information Center Cameron Station Alexandria, VA 22304-6145	2
2.	Library, Code 0142 Naval Postgraduate School Monterey, CA 93943-5002	2
3.	Commandant of the Marine Corps Code TE06 Headquarters, U.S. Marine Corps Washington, D.C. 20380-0001	1
4.	Weapons Engineering Curricular Office, Code 33 Spanagel Hall, Room 328 Naval Postgraduate School Monterey, CA 93943-5100	1
5.	Naval Engineering Curricular Office, Code 34 Department of Mechanical Engineering Naval Postgraduate School Monterey, CA 93943-5100	1
6.	Prof. A. J. Healey, Code ME/HY Chairman Department of Mechanical Engineering Naval Postgraduate School Monterey, CA 93943-5100	1
7.	Prof. A.G. Fox, Code ME/FX Department of Mechanical Engineering Naval Postgraduate School Monterey, CA 93943-5100	3
8.	Prof. Terry R. McNelley, Code ME/MC Department of Mechanical Engineering Naval Postgraduate School Monterey, CA 93943-5100	1
9.	Dr. D.J. Michel, Code 6000 Naval Research Laboratory Washington, DC 22375	1

10. Dr. George Yoder, Code 11 — 1
Office of Naval Research
Balston Towers
Arlington, VA 21043

11. Capt. Scott Fuller, USMC — 1
Weapons and Systems Engineering Department
U.S. Naval Academy
Annapolis, MD 21402-5025

12. Lt. C.E. Whitman, USN — 1
924 Florida Avenue (#B-14)
Panama City, Fl 32404

13. Lt. E.F. Goodson, Sr. — 1
SWOSCOLCOM-DH CSE 112
Newport, RI 93943-5100

14. Capt. Wang Te-Kang (Taiwan Army) — 1
SMC #1904
Naval Postgraduate School
Monterey, CA 93943-5100

15. LT. Steve Cade, USN — 1
SMC #1130
Naval Postgraduate School
Monterey, CA 93943-5100